Hadronic structure on the light front. IV. Heavy and light baryons

Edward Shuryak[*] and Ismail Zahed[†]

Center for Nuclear Theory, Department of Physics and Astronomy, Stony Brook University, Stony Brook, New York 11794–3800, USA

(Received 15 August 2022; accepted 12 January 2023; published 24 February 2023)

This work is a continuation in our series of papers that addresses quark models of hadronic structure on the light front. The chief focus of this paper is the quantum-mechanical solution of the three-quark model Hamiltonian describing baryons. In Jacobi coordinates, we use a harmonic oscillator basis for the transverse directions. For the longitudinal momentum fractions x_i, the pertinent basis follows from quantum mechanics in a "triangular cup" potential, which we solve exactly. We calculate the masses and light-front wave functions for the flavor symmetric $\frac{3}{2}^+$ baryons bbb, ccc, sss, uuu.

DOI: 10.1103/PhysRevD.107.034026

I. INTRODUCTION

Since this is the fourth paper of the series [1–4], it does not need an extensive introduction. Its main goal is to bridge the gaps between subfields of hadronic physics, with our general direction being from (i) the vacuum structure in its Euclidean formulation (instantons and lattice), to (ii) the hadronic structure and quark-quark interactions and resulting spectroscopy, to (iii) the hadronic structure on the light front with its novel Hamiltonians and wave functions.

The connection between (i) and (ii) is provided by nonlocal gauge field correlators, such as e.g. correlations of Wilson lines defining static quark potentials. Using lattice or semiclassical models of the vacuum fields, one can evaluate them. The connection between (ii) and (iii) is less developed, as neither spectroscopists nor people studying partonic observables were inclined to study them. (The former community is now living through a deluge of new hadrons discovered lately, and is rather busy.) So, let us emphasize some of the reasons for its development.

Standard spectroscopy [in the center-of-mass (c.m.) frame] uses rather different tools for states made of heavy and light quarks. The differences stem from both kinematical and dynamical reasons.

Kinematically, the heavy quarkonia can be treated nonrelativistically, using the Schrödinger equation and perturbative effective theories like perturbative Heavy Quark QCD, while the light quarks are studied with relativistic tools such as the Bethe-Salpeter equation and the like. (In fact, even the standard approaches to heavy quarkonia are not so accurate, as one might get from textbooks. Say, for charm quark, the typical velocity is not really small, $v \sim \frac{1}{2}$ or so.)

Dynamically, there are important differences between heavy and light quark interactions. Indeed, light quark physics is tightly bound to the issue of chiral symmetry breaking and its root causes—strong short-range effects described by Nambu and Jona-Lasinio (NJL) operators or instanton-based 't Hooft Lagrangians. Most of that was well understood in the 1990s and need not be repeated here.

However, as we have shown in [1], a dilute instanton ensemble is only one part of the vacuum fluctuations related with gauge topology at low resolution, and when one studies gauge field observables one finds larger effects at moderately higher resolution. Even for heavy quarkonia, we argued that a "dense vacuum" with instanton–anti-instanton pairs (incomplete tunneling through a topological barrier) contributes to Wilson line correlators, with and without magnetic fields, and generates a significant (if not dominant) fraction of the central and spin-dependent forces. This raises a question of how one can include those effects for light quarks.

Fortunately, both of these kinematical and dynamical issues are much less severe on the light front. The kinematics in this case is fully relativistic for all masses. There are no sudden changes, as one goes from heavy to light quarks. Quark masses enter the H_{LF} in a very uniform way and (as we have shown in the previous papers of the series [1–3]), one can consistently derive the mesonic properties from $\bar{b}b$ to light $\bar{q}q$ by the same tools. Indeed, in the first approximation, the transverse oscillator Hamiltonian generates near-linear Regge dependences of M^2 on the principal quantum number n and angular momentum m. Dynamical issues also get less severe. In particular, on the light front,

[*]edward.shuryak@stonybrook.edu
[†]ismail.zahed@stonybrook.edu

Published by the American Physical Society under the terms of the Creative Commons Attribution 4.0 International license. Further distribution of this work must maintain attribution to the author(s) and the published article's title, journal citation, and DOI. Funded by SCOAP[3].

even light quarks can be "eikonalized" as they move along approximately straight lines.

A. Single-flavor baryons

Baryons are just another application of the tools developed along the lines mentioned above, but this time for three-quark systems. There are important technical issues here as well, as the barrier between "relative motion" in mesons and baryons is due to the differences between the obvious variables describing the relative motion of two particles, and the nontrivial choices of variable for few-body quantum mechanics. We will address those below, but before that let us add some general remarks.

In principle, another (nontechnical) issue is related with the so-called "color junction" of three strings. The quadratic confining potential of a "star" (or Y) model fixes the junction at the origin, with no dynamics. For static potentials we can probe the effects of the junction by changing its location. However, the junction is in general dynamical, and should be treated as a *fourth body*. In general, the effective string Lagrangians carry also boundary terms, and a junction line connecting the three world volumes should also be added as a boundary contribution. The dynamics of the junction can only be ignored if it is heavy, but in so far as there is no empirical indication of that. This problem remains to our knowledge open.

This not withstanding, one should note that in the last decade, we have seen discoveries of multiple new hadrons in the so-called heavy-light sector, including QQq baryons and tetraquarks of the type $\bar{Q}Qq\bar{q}$ and $QQ\bar{q}\,\bar{q}$. Calculations for similar states with five and six quarks are ongoing by many groups. They will shed more light on the issue of quark-quark interactions. Also, baryons too have a five-quark sector, responsible for the *antiquark sea*, well studied experimentally in the case of the proton and neutron. Their flavor structure has been recently discussed by one of us [5].

Nonrelativistic and semirelativisitc constituent quark models, have been developed since the 1960s, and they exist in numerous versions. One well-documented (and still widely used as a reference point) approach is that by Isgur and Karl [6], which was updated for heavy quark states, see e.g. [7]. These authors treated confinement by an oscillatory potential, which methodically will turn out to be similar to our H_{LF} (but for squared mass, not energy). A well-known problem with the model is its predictions of many more baryonic states than what was experimentally observed.

The focus of this paper is on basic baryons which are completely symmetric in flavor, such as $\Delta^{++}_{uuu}, \Omega^{-}_{sss}$, $\Omega^{++}_{ccc}, \Omega^{-}_{bbb}$. Only the first two of them have been observed. (According to estimates, Ω^{++}_{ccc} will be discovered in the next LHC run.) The reason is that flavor asymmetric pairs such as $ud, us, ds\ldots$ have deeply bound diquark correlations which will be the subject of our next paper [4].

General considerations for these hadrons are well known, e.g. summarized in the early note by Bjorken [8].

TABLE I. Baryon masses and binding energies (all in GeV) for different quark flavors. Two baryon masses in the last two rows are experimental; all other numbers are as used in Ref. [7].

	m_Q	$M^{3/2^+}_{QQQ}$	$M^{3/2^+}_{QQQ} - 3m_Q$
b	5.2019	14.834	−0.7717
c	1.8182	4.965	−0.4896
s	0.5553	1.672	0.006
q	0.2848	1.232	0.3776

If the color part of the wave function is antisymmetric and the flavor part is symmetric, then Fermi statistics requires the spin-orbital part to be symmetric as well. The simplest one, with no orbital motion, then fixes spins to be e.g. ↑↑↑ and the global quantum number to be $\frac{3}{2}^+$. We will focus on the sector with zero orbital momentum, thereby avoiding the inclusion of spin-orbit mixing (on which we focused on in the previous paper [3] for mesons).

In Table I we show the quark and baryon masses, as well as the binding of the lowest $\frac{3}{2}^+$ states according to Ref. [7]. We note that as we move from heavy to light baryons, the binding changes from negative to positive values (relative to the sum of the masses). This is due to the attractive Coulomb interaction at small distances, whose role dramatically decreases for lighter quarks, as their states become larger in size.

The dependence of the masses and wave functions of these *ground state* baryons, on the quark mass is of course only one issue to be considered. Another is their spectrum, in particular the dependence on the principle quantum numbers n and total angular momentum J. It is well known that confining strings lead to specific Regge trajectories, both for mesons and baryons. For example, we show in Fig. 1 that the squared masses of various Δ resonances follow linear trajectories, versus angular momentum J. Two further remarkable observations are (i) both plots have the same slope, and (ii) this slope is the same as for mesons. This leads to the well-known difficulty of a star (or Y) and other stringy models: they do not yield the correct Regge slope, as the tension of three strings is different from that of a single string in mesons. The qualitative resolution of this difficulty for the nucleons is believed to be a quark-diquark configuration, with a single string between them. However, a dynamical justification of such a configuration for $J = 3/2$ baryons is still missing, especially as a function of the radial quantum number n. Needless to say, we do not yet have experimental information on many sss and any ccc baryons.

We start the paper by addressing the static three-quark potentials, and by evaluating these potentials from the instanton liquid view of the vacuum fields. The results obtained will be compared to those calculated on the lattice, with rather good agreement as we will show. However, for relevant distances these potentials do not agree with the popular stringy Y and V models, but are closer to the so-called "Ansatz A," with half binary string interactions.

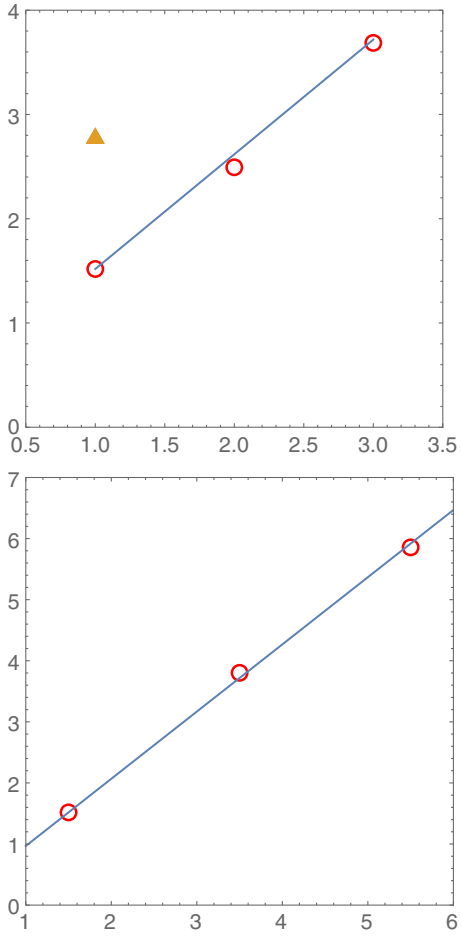

FIG. 1. Top: red circles are the squared masses of Delta resonances $M^2_\Delta(n+1,3/2)$ $(\mathrm{GeV})^2$ from PDG tables versus the principle quantum number $n+1=1,\ 2,\ 3$. The brown triangle corresponds to the triple-strange baryon $M^2_\Omega(1,\frac{3}{2})$. The lower plot shows the dependence of the Delta resonances $M^2_\Delta(1,J)$ with angular momenta $J=\frac{3}{2},\frac{7}{2},\frac{11}{2}$. Both straight lines have the same slope 1.1 GeV^2.

This notwithstanding, we still proceed to the light-front Hamiltonian, starting from a basic stringy pictures as in the Y and V models. Following our analysis of the mesons in [2], we derive and solve the light-front Hamiltonian H_{LF} for baryons, by including the kinetic and confining terms only. We will use Jacobi coordinates, exactly excluding the spurious c.m. motion, with the ensuing quantum mechanics in six dimensions. We will use the momentum representation, in which the kinetic and potential terms exchange roles. The physical domain of the longitudinal momenta will be certain triangles. As we will show, quantum mechanics on such manifolds is nontrivial but solvable.

II. THREE-QUARK POTENTIALS

A. Simplified models

We start by enumerating the stringy models discussed in the literature.

(1) Y model: The simplest baryon configuration following from the quarkonium Cornell potential consists of a perturbative Coulomb term plus a linear string potential. This is the Y (or star) model, with three strings going from quarks to a certain point where the "string junction" is located.

(2) V model: In the V model one of the quarks sits directly on the color junction, and therefore there are only two strings in a baryon.

(3) A model: This is a somewhat mysterious model, which is nevertheless widely used by spectroscopists. We will call it model A as it corresponds to the following Ansatz:

$$V_A=\frac{1}{2}(V_{q\bar{q}}(r_{12})+V_{q\bar{q}}(r_{13})+V_{q\bar{q}}(r_{23})) \quad (1)$$

in which $V_{q\bar{q}}(r_{12})$ is the usual quarkonium potential, summed over all three pairs. Its mysterious element is the factor $(1/2)$ in front, separating it from the so-called Δ model. It is justified at small distances, as the ratio of the perturbative color Casimir for $q\bar{q}$ and qq pairs in baryons. At large distances, the potential is nonperturbative, and (1) subsumes Casimir scaling.

Theoretical arguments using the vortex piercing picture of confinement have been given to support it [9], which carry also to large N_c

$$\frac{1}{2}\to\frac{1}{N_c-1}$$

much like the one-gluon exchange. Indeed, we know on general ground that for $N_c=2$, mesons and diquarks should have the same potential. Also, for large N_c, the qq force is down by $1/N_c$ in comparison to the $q\bar{q}$ force. So perhaps this factor is in fact correct for *all* nonperturbative effects.

These models provide certain predictions which vary depending on the geometry of the three quark locations. We will discuss those as we proceed, and compare them with both numerically obtained potentials from lattice simulations, as well as with our calculations using a "dense instanton liquid" vacuum model.

B. Lattice three-quark potentials at large distances

If three quarks are *static*, their interaction can be evaluated using the correlators of three Wilson lines

$$\langle \mathbf{1}-\mathbf{W}(\vec{r}_1)\mathbf{W}(\vec{r}_2)\mathbf{W}(\vec{r}_3)\rangle \sim e^{-V(\vec{r}_1,\vec{r}_2,\vec{r}_3)\tau}$$

running in the Euclidean time direction. In the case of quarkonia the color indices in $\langle \mathbf{W}\mathbf{W}^\dagger\rangle$ can either be convoluted in a single trace or a double trace (Polyakov loops). The six color indices in $\mathbf{W}$ (not shown) can be

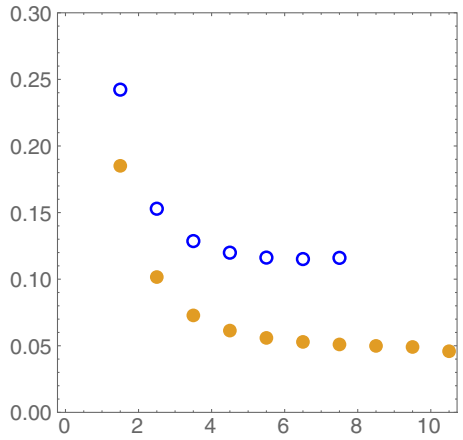

FIG. 2. Forces dV/dx versus x in lattice units, calculated from the lattice potentials as in [10]. The open points are for an equilateral triangle, and the closed points are for a linear quark-diquark setting (the same as the standard quark-antiquark one).

convoluted in many more ways, and sandwiched with the initial and final color wave functions of the baryon $\sim\epsilon^{abc}$. If the Euclidean time τ is infinitely long, they should all lead to the same potential.

The three-quark static potentials have been assessed on the lattice since the 1980s. For definiteness we will use the data compiled in the Appendix in [10] for different geometries of the quark locations. As these authors have shown, none of the models listed above provide a fully satisfactory fit to the data. Nevertheless, they contain important lessons, few of which we would like to formulate in this section.

The three static quarks can be arranged in triangles of different sizes and shapes. Let us start with the most symmetric setting, the *equilateral* triangle. Following [10], three quarks are assigned to points $(x,0,0)$, $(0,x,0)$, $(0,0,x)$, and will be characterized by this distance x. All three sides are $\sqrt{2}x$, but all plots below will be given as a function of x.

Furthermore, let us focus on the large-x limit, for which the differences between models is most obvious. In order to exclude constant terms (possibly depending on the triangle geometry), we plot in Fig. 2 the forces dV/dx rather than the potentials. They are compared to the quark-diquark potential (coinciding with the quarkonium potential as shown in the same paper). Indeed, at large distances the forces asymptote constants.

[This is expected for confining flux tubes. However, in the real world (or lattice simulations with dynamical quarks) we expect "avoided crossing phenomenon" to happen, whereby sufficiently long flux tubes break by production of a light quark-antiquark pair, so that the growing potential turns into a constant at large distances. In fact, the real situation is more complex, as was understood long ago for crossing of molecular levels: as shown by Landau, Zener and others in 1932, the probabilities to follow or switch levels depend on the velocity with which the crossing is approached. The more general issue of mixing between baryons and pentaquarks is being discussed in spectroscopy. Using light-front wave functions (LFWF), one of us [5] evaluated this mixing in order to calculate PDFs of "sea antiquarks." In this paper we will ignore the level crossing in the potentials.]

The constants in front of the linear terms depend on the geometry of the quark locations, and are different for different models. We will discuss three models and three geometries in the next subsection. Here, we start with the well-known Y model, with three strings going from the quarks to the center of mass of the triangle, where the "string junction" is located. In this model the force should be three times the string tension times the ratio of the distance to the center in units of x. For an equilateral triangle it is

$$\frac{dV_Y}{dx} = 3\sigma\sqrt{\frac{2}{3}} = \sqrt{6}\sigma. \tag{2}$$

In the V model, one of the quark sits directly on the color junction. In this case there are *two* strings rather than three. For the particular triangle under consideration, we have

$$\frac{dV_V}{dx} = 2\sigma\sqrt{2} = \sqrt{8}\sigma. \tag{3}$$

Finally, for the A model, we have the smallest force

$$\frac{dV_A}{dx} = \frac{1}{2}3\sigma\sqrt{2} \tag{4}$$

with $\sigma_A/\sigma_Y \approx 0.866 < 1$, whatever the triangular configuration.

In Fig. 2 the filled points correspond to the string tension σ for a quark-diquark (identical to quark-antiquark) using the same lattice configurations. For the Y-mode, the ratio is

$$\frac{\sigma}{\sigma_Y} = \frac{\sigma}{\sqrt{6}\sigma} \approx 0.854 \tag{5}$$

instead of 1. For the V model we have $\sqrt{8/6} \approx 1.15$, which is even larger. In the A model, it is comparable to σ

$$\frac{\sigma}{\sigma_A} \approx \frac{0.854}{0.866} \approx 1. \tag{6}$$

The first lesson about the three-quark lattice potentials is that the string-based Y, V models overpredict the forces at large distances, while the ansatz A model reproduces the force (for an equilateral triangle). Of course, we should consider other geometries, and probe intermediate distances as well, before ruling it as a successful model for the three-quark potential.

The second lesson is that some geometries are better for model separation than others. Indeed, another triangular limit in which one corner is far from the two others (including the quark-diquark picture) yields a single string tension times the longest distance for model Y, which is the same as half the string tension times the two longest distances for model A.

C. Three-quark static potentials from the instanton vacuum

Before proceeding to the static three-quark potentials from the three models presented earlier, using instantons, we first put forth a few remarks that suggest why model A would be favored.

It is a very important issue in the theory of few-body quantum states (e.g. in nuclear physics tritium and He^3) to separate effects of well-constrained two-body forces from "truly three-body" ones, which are then extracted from fits to experiment. In baryons made of three quarks, we first observe that the color wave function ϵ^{abc} involves all three colors, while the instanton fields are $SU(2)$ valued in the space of three colors. This suggests that the main potential is best approximated by binary potentials. Among the models we presented, only Ansatz A (1) has such a form.

Furthermore, since the instanton fields do not generate confinement, the pertinent potentials asymptote constants for the binary potential $V(r_{ij}\to\infty)=2\Delta M$, and for the triple potential $3\Delta M$, etc. Since there are three binary potentials, these large distance limits can only be reconciled if there is a factor $(1/2)$ in front, as in Ansatz A.

The instanton-induced potentials between three static quarks can be computed using the same expressions for Wilson lines as was traditionally used for a binary potential. The $SU(2)$ part of the Wilson line can be expressed using Pauli (rather than Gell-Mann) matrices τ^i

$$\mathbf{W}^a_{lb}=(c_l\mathbf{1}-i(\vec{\tau}\cdot\vec{n}_l)s_l)^a_b,\qquad a,b=1,2;l=1,2,3 \quad (7)$$

with trigonometric functions involving color rotation angles that depend on the 3D distances $\vec{\gamma}_i, i=1,\ 2,\ 3$ between the location of Wilson lines $\vec{r}_i$, and the instanton center $\vec{z}$

$$\begin{aligned} c_i &\equiv \cos\left(\pi-\frac{\pi\gamma_i}{\sqrt{\gamma_i^2+\rho^2}}\right),\\ s_i &\equiv \sin\left(\pi-\frac{\pi\gamma_i}{\sqrt{\gamma_i^2+\rho^2}}\right),\\ \gamma_i^2 &= (\vec{r}_i-\vec{z})^2,\qquad \vec{n}_i=\vec{\gamma}_i/|\vec{\gamma}_i|. \end{aligned} \quad (8)$$

We note that at large distances $|\gamma_i|\gg\rho$, the phases vanish. At small distances they go to π, with cosines set to -1, with a flipped quark color direction. Since a standard instanton does not act on a quark with the third color, this 2×2 matrix should be extended trivially (by 1) to 3×3.

To properly model the color-isotropic vacuum, one should include some random $SU(3)$ matrices U which rotate the instanton fields from their standard $SU(2)$ plane, to an arbitrary plane in $SU(3)$. These matrices should then be averaged using the Haar measure of the SU(3) group (see Appendix A for more details)

$$\int dU(U^{a_1}_{i_1}\mathbf{W}^{i_1}_{1j_1}U^{\dagger j_1}_{b_1})(U^{a_2}_{i_2}\mathbf{W}^{i_2}_{2j_2}U^{\dagger j_2}_{b_2})(U^{a_3}_{i_3}\mathbf{W}^{i_3}_{1j_3}U^{\dagger j_3}_{b_3}). \quad (9)$$

For the instanton-induced potential we thus get the following expression:

$$\begin{aligned} V=\frac{2n_{I+\bar{I}}}{N_c}\int d^3z\Bigg[&(1-c_1c_2c_3)\delta^{a_1}_{b_1}\delta^{a_2}_{b_2}\delta^{a_3}_{b_3}\\ &+\frac{N_c^2}{(N_c^2-1)}c_1s_2s_3n_2\cdot n_3\delta^{a_1}_{b_1}\left(\frac{1}{2}\lambda^B_2\right)^{a_2}_{b_2}\left(\frac{1}{2}\lambda^B_3\right)^{a_3}_{b_3}\\ &+2\ \text{perm.}\Bigg] \end{aligned} \quad (10)$$

where $n_{I+\bar{I}}$ is the 4D instanton plus anti-instanton density. This is valid for any color states of the three quarks. For a color singlet three-quark baryon, one can either use its antisymmetric wave function $\sim\epsilon^{abc}$, or set the quark colors as $a_1=b_1=1, a_2=b_2=2, a_3=b_3=3$.

The results of the calculation of the instanton-induced potentials, for the preceding three triangular shapes, are shown as filled circles in Fig. 3. The instanton size was taken to be the usual $\rho=\frac{1}{3}$ fm, and the density parameter $\kappa=\pi^2n_{I+\bar{I}}\rho^4=1$ (dense instanton liquid). So the calculation has only one additive free parameter, which we have set by requiring all potentials to vanish for small triangles. One can see that the shape of the potentials and their magnitude are rather independent of the shape of the triangles. In all cases the potential at large x becomes close to $3\Delta M$, for three independent quarks.

The potential is plotted in Fig. 3 versus x defined via quark positions as follows (same as on the lattice):

$$r_i=(x,0,0)(0,x,0),(0,0,x)\quad\text{equilateral,} \quad (11)$$

$$r_i=(x,0,0)(0,x,0),(0,0,0)\quad\text{direct,} \quad (12)$$

$$r_i=(x,0,0)(0,a,0),(0,0,a)\quad\text{long.} \quad (13)$$

In the plots, the dashed and solid straight lines refer to the linear predictions of the models V and A, discussed at the beginning of this section, respectively. They correspond to

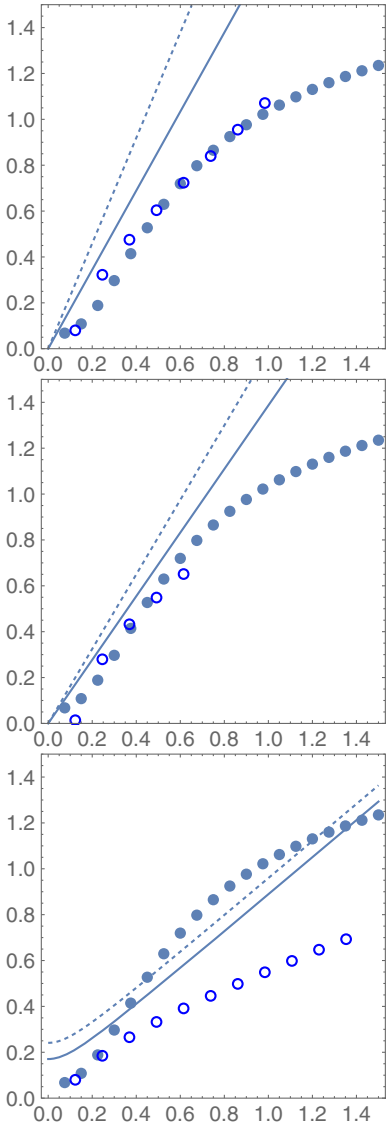

FIG. 3. The three-quark potentials V (GeV) versus x (fm) defined in (11), for equilateral, direct, and long triangles, top to bottom. The open points correspond to lattice simulation, the closed points to our calculation in the dense instanton liquid model. Linear predictions of the models V and A are shown by the dashed and solid lines, respectively.

$$
\begin{aligned}
&V_V = \sqrt{8}\sigma x, \qquad V_A = \frac{3}{\sqrt{2}}\sigma x \quad \text{equilateral},\\
&V_V = 2\sigma x, \qquad V_A = \sigma x(1+1/\sqrt{2}) \quad \text{direct},\\
&V_V = \sigma(\sqrt{x^2+a^2}+a\sqrt{2}),\\
&V_A = \sigma(\sqrt{x^2+a^2}+a/\sqrt{2}) \quad \text{long}.
\end{aligned} \tag{14}
$$

Since the constants in the potentials are not well defined, Eq. (14) are shown for comparison to the "force" (the slopes) with the instanton-induced (filled circles) and lattice potentials (open circles). Note that here we used the "empirical" string tension $\sigma = (0.4\ \text{GeV})^2$, deduced from the Regge slope α'. The corresponding lattice value is smaller by as much as 30% (perhaps due to the limited size of the lattice, or other uncertainties in the scale). Within this accuracy range, we conclude that the slope predicted by model A is in *crude agreement* with the instanton-induced potentials.

The open circles in these plots are from the lattice simulation tables in [10]; the lattice site size is $a = 0.123$ fm. Since a pointlike charge energy requires renormalization, we also shifted them downward by a constant. One can see that the instanton-induced and lattice potentials agree quite well for two former triangles, but for the "long" one even the slope does not agree. Note however that (i) the smallest side of the triangle in this case is not growing with x but remains constant and small $\sqrt{2a} = 0.174$ fm, and (ii) that this potential goes roughly to $2\Delta M$ rather than $3\Delta M$ as in the other cases. The lattice seems not to resolve the quark pair at this distance, while our continuous instanton formulas do. To resolve the issue one perhaps needs an instanton model with a realistic size distribution, and also finer lattices.

In conclusion, good agreement is shown between the instanton-induced and lattice potentials for large-enough triangles, but not for long ones. Of all the three models Y, V, A discussed, model A seems to be closer to the evaluated instanton-induced potentials, even for long geometry.

III. PRELIMINARIES

A. Jacobi coordinates

The LFWFs for baryons discussed in literature so far consider quarks as independent, so those are a function of nine coordinates (or nine momenta). The spurious c.m. motion is implicitly present: in some cases the corresponding energy is subtracted, but corrections to the wave functions are simply ignored.

However, there is no need for this. Exact kinematics with appropriate conditions can be satisfied by a well-known change of variables, widely used in many few-body applications. Total momentum is subject to three conditions,

$$
\begin{aligned}
\vec{p}_\perp^{\,\text{tot}} = \vec{p}_{1\perp} + \vec{p}_{2\perp} + \vec{p}_{3\perp} = 0,\\
x_1 + x_2 + x_3 = 1,
\end{aligned} \tag{15}
$$

so the system is in fact six-dimensional.

The main idea of the approach we use is to work in momentum representation, with the kinetic term of the Hamiltonian treated as a "potential," and the confining part (in which coordinates are used as derivative over momenta $\vec{r}_i = i\partial/\partial\vec{p}_i$) as our analogue of the "kinetic" energy.

For transverse momenta we introduce two (slightly modified) Jacobi momenta variables

$$\vec{p}_{\rho\perp}=\frac{1}{\sqrt{2}}(\vec{p}_{1\perp}-\vec{p}_{2\perp}),\quad \vec{p}_{\lambda\perp}=\frac{1}{\sqrt{6}}(\vec{p}_{1\perp}+\vec{p}_{2\perp}-2\vec{p}_{3\perp}) \tag{16}$$

in terms of which

$$\begin{aligned}\vec{p}_{1\perp}&=(\sqrt{6}\vec{p}_{\lambda\perp}+3\sqrt{2}\vec{p}_{\rho\perp})/6,\\ \vec{p}_{2\perp}&=(\sqrt{6}\vec{p}_{\lambda\perp}-3\sqrt{2}\vec{p}_{\rho\perp})/6,\\ \vec{p}_{3\perp}&=-\sqrt{6}\vec{p}_{\lambda\perp}/3.\end{aligned} \tag{17}$$

Now the total transverse momentum $\vec{p}_{\rm tot}=\vec{p}_1+\vec{p}_2+\vec{p}_3$ vanishes automatically.

The longitudinal momentum fractions are defined similarly,

$$\begin{aligned}x_1&=(\sqrt{6}\lambda+3\sqrt{2}\rho+2X)/6,\\ x_2&=(\sqrt{6}\lambda-3\sqrt{2}\rho+2X)/6,\\ x_3&=(-\sqrt{6}\lambda+X)/3.\end{aligned} \tag{18}$$

Note that $X=x_1+x_2+x_3$: unlike in the transverse direction for which $X=0$, here X should be set to 1. Therefore, the physical domain is the three-dimensional cube $x_i\in[0,1]$ *cut by a plane* $X=1$, leaving as a physical domain a triangle in λ, ρ coordinates inside which the parton fractions are all positive $x_i>0$. The three corners of the triangles correspond to parton configurations with one quark with its fraction being 1, and the two others zero. The longitudinal part of the LFWF should therefore be defined *on this triangle*.

After the wave functions in momentum representation are defined, one can reconstruct their versions in coordinate representations by the usual Fourier transform. The coordinates conjugated to $\vec{p}_\rho,\vec{p}_\lambda$ will be referred to as $\vec{r}_\rho,\vec{r}_\lambda$.

The confining part of the Hamiltonian in its simplest form can be rewritten using the einbein trick used in [2,3] and reiterated for the reader in Appendix B. For the Y (or star) model this amounts to

$$\begin{aligned}\sigma_T(|\vec{r}_1|+|\vec{r}_2|+|\vec{r}_3|)&\to\frac{\sigma_T}{2}\left(\frac{3}{a}+a(\vec{r}_1^{\,2}+\vec{r}_2^{\,2}+\vec{r}_3^{\,2})\right)\\ &\to\frac{\sigma_T}{2}\left(\frac{3}{a}+a(\vec{r}_\lambda^{\,2}+\vec{r}_\rho^{\,2})\right)\end{aligned} \tag{19}$$

with all einbein parameters set equal to a by saddle point. For Ansatz A (1) this amounts to

$$\begin{aligned}\frac{\sigma_T}{2}(r_{12}+r_{23}+r_{13})&\to\frac{\sigma_T}{4}\left(\frac{3}{a}+a(r_{12}^2+r_{23}^2+r_{13}^2)\right)\\ &\to\frac{\sigma_T}{4}\left(\frac{3}{a}+3a(\vec{r}_\lambda^{\,2}+\vec{r}_\rho^{\,2})\right).\end{aligned} \tag{20}$$

Note that when a is to be eliminated by minimization, the minimum is at $a^*=\sqrt{3/(r_\lambda^2+r_\rho^2)}$ in (19), but $a^*=\sqrt{1/(r_\lambda^2+r_\rho^2)}$ in (20). Substituting those values back to original expressions, one finds that confining potentials in (19) in Jacobi coordinates is the same as (20) after the following rescaling of the string tension:

$$\sigma_T\to\frac{\sqrt{3}}{2}\sigma_T. \tag{21}$$

Note that the rescaling factor $\frac{\sqrt{3}}{2}\approx 0.866<1$, so the tension (and thus all baryonic masses) corresponding to model A are lower than in model Y, as expected.

The quantum replacement

$$\vec{r}_\lambda\to i\frac{\partial}{\partial\vec{p}_\lambda},\qquad \vec{r}_\rho\to i\frac{\partial}{\partial\vec{p}_\rho}$$

yields a 6-D Laplacian in $\vec{p}_\lambda,\vec{p}_\rho$, for both Y and A models. The kinetic term contains the sum of corresponding momenta squared: so, in this approximation, there appears 6-D spherical symmetry in Jacobi coordinates.

B. Relativisitic semiclassical quantization in the rest frame

Before we move to the light front, however, we present our preliminary study of the problem in the rest frame. We will present in detail the Y or star configuration, with three strings connected to a junction. The junction will be assumed static and located in the c.m. for equal masses. The results for model A will be briefly quoted. In the rest frame the baryon with zero orbital momentum is spherically symmetric.

Heavy quarks can be treated via the Schrödinger equation, but for light quarks their effective masses and momenta are comparable, so nonrelativistic approximation is invalid. This distinction however can be avoided in the semiclassical approach we will use here (and of course the light-front approach is the same for light and heavy quarks). The Hamiltonian for the Y configuration is

$$H=\frac{1}{2m}(\vec{p}_\lambda^{\,2}+\vec{p}_\rho^{\,2})+\sigma_T\sum_{i=1}^{3}|\vec{r}_i|+\left(\frac{3}{2}\frac{m_Q^2}{m}+\frac{3}{2}m\right). \tag{22}$$

Here m_Q is the quark mass, σ_T the string tension, and $m=1/2e$ is the variational effective mass, arising from the einbein trick used to unwind the relativistic square root. A similar Hamiltonian was obtained in [11], using a different world-sheet embeding than the one we will present below [see (38)]. For the confining part, (19) gives

$$\sigma_T \sum_{i=1}^{3} |\vec{r}_i| \to \sqrt{3}\sigma_T (\vec{r}_\lambda^{\,2} + \vec{r}_\rho^{\,2})^{\frac{1}{2}}, \tag{23}$$

Eq. (22) simplifies to that of *one* particle in a $D = 6$-dimensional space,

$$\begin{aligned} H \to & \frac{1}{2m}(\vec{p}_\lambda^{\,2} + \vec{p}_\rho^{\,2}) \\ & + \sqrt{3}\sigma_T (\vec{r}_\lambda^{\,2} + \vec{r}_\rho^{\,2})^{\frac{1}{2}} + \left(\frac{3}{2}\frac{m_Q^2}{m} + \frac{3}{2}m\right) \\ \to & \frac{p_\mu^2}{2} + \tilde{\sigma}_T |Z_\mu| + \left(\frac{3}{2}\frac{m_Q^2}{m} + \frac{3}{2}m\right) \end{aligned} \tag{24}$$

and (24) describes a nonrelativistic and linearly confined particle of variational mass m, with coordinates $Z_\mu = (\lambda^i, \rho^i)$ in $D = 6$ dimensions as per the last relation. We have rescaled the coordinate $\sqrt{m}Z \to Z$ and string tension $\tilde{\sigma}_T = \sqrt{3}\sigma_T/\sqrt{m}$ for convenience.

An estimate of the mass spectrum can be obtained using the WKB approximation,

$$\int_{r_S}^{r_L} dr \left(2E - 2\tilde{\sigma}_T r - \frac{l(l+D-2)}{r^2}\right)^{\frac{1}{2}} = \left(n + \frac{1}{2}\right)\pi \tag{25}$$

with the end points $r_{L,S}$ solution to the cubic equation

$$2\tilde{\sigma}_T r^3 - 2Er^2 + l(l + D - 2) = 0.$$

For zero orbital motion $l = 0$, the WKB radial energy levels can be found to be

$$E_{n0}(m) = \left(\frac{3\pi}{2\sqrt{2}}\right)^{\frac{2}{3}} \left(n + \frac{1}{2}\right)^{\frac{2}{3}} \tilde{\sigma}_T^{\frac{2}{3}} \equiv \frac{\tilde{E}_{0n}}{m^{\frac{1}{3}}}. \tag{26}$$

Once combined with the extra terms in (24), we can carry the minimization in m, and set its value at the minimum. The ensuing WKB radial mass spectrum of the star baryon M_{n0} in the rest frame Reggeizes for large n *linearly*

$$\alpha' M_{n0}^2 \approx 2\sqrt{3}n \tag{27}$$

with $\alpha' = 1/2\pi\sigma_T$. We recall that the meson Regge trajectory is $\alpha' M^2 = 1$. So, in the same units our star-shaped baryons have a slope $2\sqrt{3} \approx 3.46$, compared to the mesons. It is close but not equal to the number 3, naively corresponding to the number of strings. This WKB radial Regge trajectory calculated in the rest frame has similar but not identical slope to that derived from the light front [see (61) below].

For large orbital excitations l, the motion is classical, and an estimate can be obtained by noting that for the confining potential the virial theorem gives

$$E_{0l} \approx K + V = 3K = \frac{3l^2}{2R^2}$$

with $R = (l^2/\tilde{\sigma}_T)^{\frac{1}{3}}$ fixed by the force equation. After fixing m by minimization, the mass spectrum of the star baryon is seen to Reggeize linearly in large orbital momentum l as well,

$$\alpha' M_{0l}^2 \approx \frac{6}{\pi} l \tag{28}$$

with a slope $6/\pi \approx 1.91$, so the linear Reggeization is not the same in n and l. This is in disagreement with the experimental data for light baryons, as we have demonstrated above for the isobars.

The results for model A follows from those for model Y through the rescaling (21). In particular, the Reggeized trajectories in the semiclassical approximation are

$$\begin{aligned} \alpha' M_{n0}^2 &\approx 3n, \\ \alpha' M_{0l}^2 &\approx \frac{3\sqrt{3}}{\pi} l, \end{aligned} \tag{29}$$

in comparison to (27) and (28), respectively.

IV. THE HAMILTONIAN ON THE LIGHT FRONT

The kinetic part of the LF Hamiltonian has the form

$$\sum_i \frac{\vec{p}_{i\perp}^{\,2} + m_i^2}{2p_{\text{ilong}}}$$

in which the transverse and longitudinal momenta appear differently. As in our previous papers, we rewrite it in the following form:

$$\begin{aligned} & \frac{p_{1\perp}^2 + m_Q^2}{x_1} + \frac{p_{2\perp}^2 + m_Q^2}{x_2} + \frac{p_{3\perp}^2 + m_Q^2}{x_3} \\ & = 3\sum_i (p_{i\perp}^2 + m_i^2) + \sum_i (p_{i\perp}^2 + m_i^2)\left(\frac{1}{x_i} - 3\right). \end{aligned}$$

The first quadratic term in the last line leads to a *transverse oscillator*, and the second term is called a *nonfactorizable potential* $\tilde{V}$; it mixes transverse and longitudinal variables. It will be included by different methods to be defined below.

The confining part of the LF Hamiltonian is built from terms linear in coordinates. For example the Y model with three strings going to the junction at the center has a sum of linear terms

$$V_Y = \sigma_T \sum_{i=1}^{3} |\vec{r}_i|.$$

Like we did for mesons in our previous papers, we again introduce *en einbein trick* with a variational parameter a which allows us to rewrite the linear potential as a quadratic one.

Furthermore, as in our previous papers, we use the Hamiltonian in the momentum representation. Therefore the coordinate vectors are interpreted as $\vec{r} = i\partial/\partial\vec{p}$, and therefore the confining part $\sim\vec{r}^2$ will play the role normally attributed to the kinetic energy. Quadratic confinement thus leads to a second-order Schrödinger-like equation for the eigenfunctions.

The same logics is applied to the transverse and longitudinal coordinates $\vec{r}_\perp, r_{\rm long}$, so the immediate task is to write the Laplacian operator, both in Jacobi coordinates in transverse and in our curved map (35). Both tasks are performed, as explained in Appendix C.

Let us focus for now on longitudinal momenta. In variable λ, ρ, X (18) the line element defining the metric tensor in the new coordinates is diagonal and simple

$$dl^2 = d\lambda^2 + d\rho^2 + dX^2/3. \tag{30}$$

The Laplacian (which we encounter in the confining term of the Hamiltonian) in the original coordinates also takes a simple form

$$\nabla^2 = \sum_i \frac{\partial^2}{\partial x_i^2} \to \frac{\partial^2}{\partial\lambda^2} + \frac{\partial^2}{\partial\rho^2} + 3\frac{\partial^2}{\partial X^2}. \tag{31}$$

Since we work on constant $X = 1$ we need only the first two terms.

Therefore, the first problem we encounter is to define eigenfunctions of the Laplacian on the triangular physical domain in the $\lambda - \rho$ variable. As we will show below, for the equilateral triangle this problem can in fact be solved analytically.

The main difficulty is related with the nonfactorizable potential $\tilde{V}$. Its structure is schematically given by the combination

$$\tilde{V} \sim \left(\frac{1}{x_1} + \frac{1}{x_2} + \frac{1}{x_3} - 9\right), \tag{32}$$

assuming $((\vec{p}_i^{\perp})^2 + m_i^2)$ can be approximated by its average and factor out. The main feature of $\tilde{V}$ is that it is small near the center of the triangle, but becomes large at all boundaries, see e.g. its contour plot shown in Fig. 4. Therefore we call it a "triangular cup." The singular nature of $\tilde{V}$ at the boundaries leads to divergences in matrix elements, unless the wave functions vanish there. Therefore, the problem we set to solve must have Dirichlet boundary conditions $\psi_i(\lambda, \rho) = 0$ at the boundaries for all functions.

Quantum mechanics on a triangle with the potential $\tilde{V}$ will be solved below, by two numerical methods. But before we do so, it is always useful to start with a less accurate but much simpler variational method.

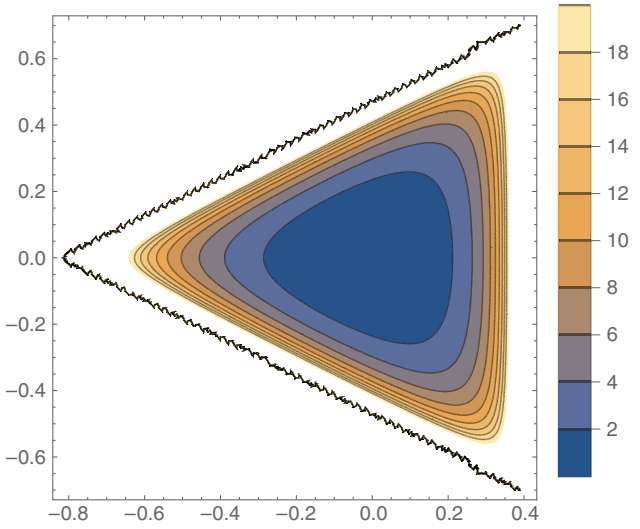

FIG. 4. The contour plot of the triangular cup potential $V(\lambda, \rho)$ on λ, ρ plot.

To exclude divergences on the boundaries, the wave function should vanish, so we simply include linear suppression factors and assume that

$$\Psi(\lambda, \rho) = \left[\prod_i x_i(\lambda, \rho)\right]\Phi(\lambda, \rho) \tag{33}$$

with some regular Φ. (This procedure is known in nuclear and condensed many-body physics, through the use of Jastrow type wave functions.) Let us then take this regular function to be a Gaussian centered in the triangle

$$\Phi(\lambda, \rho) = \exp\left(-A\left(\lambda^2 + \left(\rho - \frac{1}{\sqrt{6}}\right)^2\right)\right) \tag{34}$$

with a variational parameter A. We use (33), evaluate the average of the Laplacian and of the potential V, and plot the result as a function of A in Fig. 5. As expected, increasing A—that is making the wave function better localized near the center—leads to a growth of the mean Laplacian and a decrease of the mean V. Taking those two averages with proper coefficients, one finds a minimum of the total Hamiltonian.

A. Longitudinal momentum fractions in factorizable coordinates

The longitudinal motion can be treated in a different way, by a nonlinear maps with factorizable measure into a new set of variables. This mapping was developed in [5] for any number of constituents, in particular it was used for the three- and five-quark sectors of the baryons.

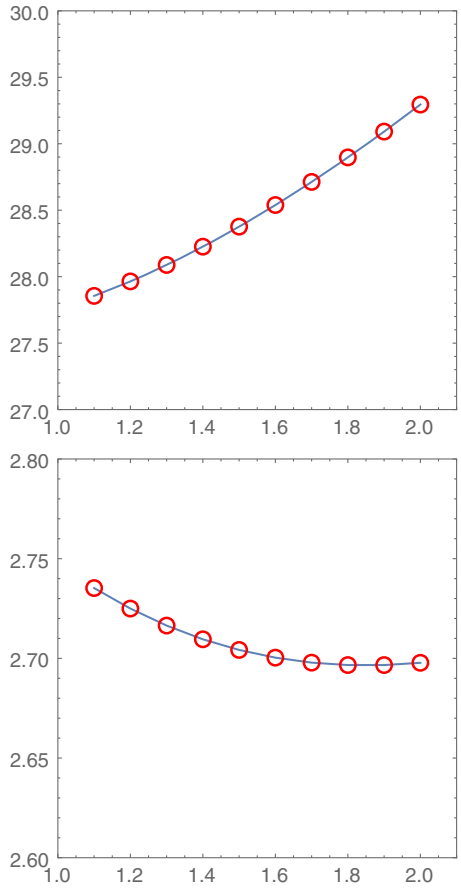

FIG. 5. The average Laplacian (top) and $V(\lambda,\rho)$ (bottom) versus the variational paremeter A. See text.

Let us parametrize the 3-momentum fractions of the quarks, using the following three parameters s, t, u:

$$x_1 = u\left(\frac{1+s}{2}\right)\left(\frac{1+t}{2}\right),$$
$$x_2 = u\left(\frac{1-s}{2}\right)\left(\frac{1+t}{2}\right),$$
$$x_3 = u\left(\frac{1-t}{2}\right). \tag{35}$$

The longitudinal momentum constraint $x_1+x_2+x_3=u$ will be enforced later $u\to 1$.

The inverse map explains better the meaning of s, t as "asymmetries,"

$$s = \frac{x_1-x_2}{x_1+x_2},$$
$$t = \frac{x_1+x_2-x_3}{x_1+x_2+x_3},$$
$$u = x_1+x_2+x_3. \tag{36}$$

The corresponding metric and Laplacian in the s, t, u coordinates are listed in Appendix D. The main point is that the physical domain of the s, t variables is a *square*, since both vary between -1 and 1. With the help of appropriate Jacobi polynomials, one can have factorized orthonormal basis functions, in terms of which the Hamiltonian matrix elements can be computed. With some model Hamiltonian (different from the one used in the present paper), the mass and wave function for the lowest Δ states have been evaluated in [5]; see Fig. 6. We show it in order to compare with the wave functions to be derived below. Note that the wave function is approximately Gaussian, with strong suppression near the edges of the physical domain. (It is rather different from that of the nucleon; see the original paper.)

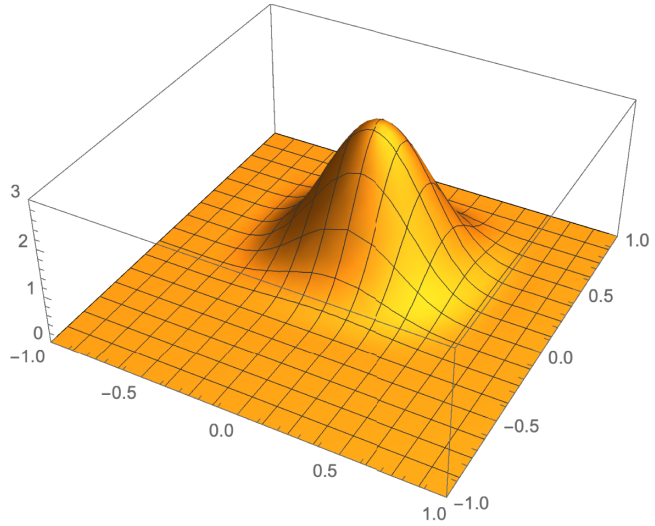

FIG. 6. The wave function of $\Delta(3/2)$ baryon, in s, t coordinates, from [5].

In this paper we will not use the s, t coordinates and the Jacobi polynomial basis. Yet we note that whatever coordinates or basis is used, one cannot simply invent a convenient Hamiltonian in those coordinates, plus whatever motivations. In particular, the Laplacian in the original coordinates should be rewritten using the pertinent expressions from differential geometry. For the s, t map given above, the Laplacian is involved and listed in Appendix C.

V. NAMBU-GOTO STRING AND CONFINEMENT

A. Confining light-front Hamiltonian

Ignoring Coulomb and spin effects, we start by focusing on confinement by a relativistic string. The action in the first quantized form can be written as

$$S[\theta] = \int_0^T d\tau \sum_{i=1}^3 \left(e_i m_i^2 + \frac{1}{4e_i}\dot{x}_i^2\right)$$
$$+\sigma_T \sum_{i=1}^3 \int_0^T d\tau \int_0^1 d\sigma_i \sqrt{\dot{X}_i^2 X_i'^2 - (\dot{X}_i\cdot X_i')^2}. \tag{37}$$

In the first term, describing end point masses, we use the einbein trick which we will use consistently throughout these papers to get rid of unwanted square roots. Note that if one performs minimization with respect to the three einbein parameters e_i, it yields back the standard free relativistic action for massive particles (in Euclidean signature).

The string world-sheet action in the Nambu-Goto action includes derivatives over internal coordinates τ, σ shown by a dot and prime, respectively. The world sheets themselves can be described by the so called "ruled surfaces," parametrized by

$$\begin{aligned} X_i^\mu(\tau,\sigma_i;\theta) &= z^\mu(\tau,\theta)+\sigma_i r_i^\mu, \\ r_i^\mu &= (r_{i\perp}, r_{i3}, 0), \\ z^\mu(\tau,\theta) &= (0_\perp, \sin\theta\tau, \cos\theta\tau), \end{aligned} \tag{38}$$

with $z^\mu(\tau,\theta)$ being the world line of the string junction. (Our notations for the coordinates are 1, 2 for transverse, 3 for longitudinal beam direction, and 4 for time.)

For baryons in the so-called star configuration, the string junction and the end points follow parallel trajectories, sloped at angle θ with respect to the 4-direction. For $\theta = 0$, the analysis corresponds to a star baryon in the rest frame. For arbitrary θ with subsequent analytical continuation $\theta \to -i\chi$, the analysis corresponds to a star baryon on the light front.

As already explained above, to factor out spurious motion of the center of mass, we use Jacobi coordinates. For equal quark masses

$$m_1 = m_2 = m_3 = m_Q,$$

the center of mass coincides with the location of the string junction z^μ. Also, although the einbeins are arbitrary and fixed only by minimization for the free part, symmetry suggests that the minima are equal or $e_1 = e_2 = e_3 = e$, with only e to minimize, by steepest descent. This will be assumed throughout.

The specific form of the Jacobi coordinates for the end points is

$$\begin{aligned} r_1^\mu &= \frac{1}{\sqrt{6}} r_\lambda^\mu + \frac{1}{\sqrt{2}} r_\rho^\mu, \\ r_2^\mu &= \frac{1}{\sqrt{6}} r_\lambda^\mu - \frac{1}{\sqrt{2}} r_\rho^\mu, \\ r_3^\mu &= -\frac{\sqrt{2}}{\sqrt{3}} r_\lambda^\mu, \end{aligned} \tag{39}$$

with a kinetic contribution

$$\int_0^T d\tau \left(3em_Q^2 + \frac{3}{4e} + \frac{1}{4e}(\dot{r_\lambda}^2 + \dot{r_\rho}^2) \right) \tag{40}$$

in (37). The Nambu-Goto string contribution is

$$\int_0^T d\tau \sigma_T \sum_{i=1}^3 |\xi_i(\theta)| \tag{41}$$

with the invariant distances

$$|\xi_i(\theta)| = (r_{i\perp}^2 + \cos^2\theta r_{i3}^2)^{\frac{1}{2}},$$

or, in the Jacobi coordinates

$$\begin{aligned} \xi_1^2(\theta) &= \frac{1}{6} r_{\lambda\perp}^2 + \frac{1}{2} r_{\rho\perp}^2 \\ &\quad + \frac{1}{6} r_{\lambda\perp}\cdot r_{\rho\perp} + \cos^2\theta \left(\frac{1}{\sqrt{6}} r_{\lambda 3} + \frac{1}{\sqrt{2}} r_{\rho 3} \right)^2, \\ \xi_2^2(\theta) &= \frac{1}{6} r_{\lambda\perp}^2 + \frac{1}{2} r_{\rho\perp}^2 \\ &\quad - \frac{1}{6} r_{\lambda\perp}\cdot r_{\rho\perp} + \cos^2\theta \left(\frac{1}{\sqrt{6}} r_{\lambda 3} - \frac{1}{\sqrt{2}} r_{\rho 3} \right)^2, \\ \xi_3^2(\theta) &= \frac{2}{3} r_{\lambda\perp}^2 + \frac{2}{3}\cos^2\theta r_{\lambda 3}^2. \end{aligned} \tag{42}$$

The full action (prior to analytical continuation) is (40) plus (41)

$$\begin{aligned} S[\theta] \to \int_0^T d\tau \Bigg(& 3em_Q^2 + \frac{3}{4e} \\ & + \frac{1}{4e}(\dot{r_\lambda}^2 + \dot{r_\rho}^2) + \sigma_T \sum_{i=1}^3 |\xi_i(\theta)| \Bigg). \end{aligned} \tag{43}$$

B. Going to the light-front frame

For $\theta \to -i\chi$ and $T \to iT_M$, (43) analytically continues to the light-front Hamiltonian or squared mass

$$H_{LF} = \sum_{i=1}^3 \left(\frac{k_{i\perp}^2 + m_Q^2}{x_i} + 2\sigma_T (|i\partial/\partial x_i|^2 + M^2 r_{i\perp}^2)^{\frac{1}{2}} \right) \tag{44}$$

with the constraints: transverse $\sum_{i=1}^3 k_{i\perp} = P_\perp = 0$ and longitudinal $\sum_{i=1}^3 x_i = 1$, with the standard momentum fractions $x_i = k_i^+/P^+$.

C. A digression to 1 + 1 space-time

The Hamiltonian derived above contains nonfactorizable interaction between the longitudinal and transverse coordinates which make the problem difficult. So, before we will address it in full, let us discuss its longitudinal part alone. The Hamiltonian (44) is then reduced to

$$H_{LF,L} = \sum_{i=1}^{3}\left(\frac{m_Q^2}{x_i} + 2\sigma_T|i\partial/\partial x_i|\right). \quad (45)$$

For a baryon in the star configuration, (66) yields a longitudinal squared mass spectrum M_n^2, and parton amplitudes $\varphi_n[x]$

$$\sum_{i=1}^{3}\left(\frac{m_Q^2}{x_i} + 2\sigma_T|i\partial/\partial x_i|\right)\varphi_n[x] = M_n^2\varphi_n[x]. \quad (46)$$

Modulo the effective string tension from the three-dimensional reduction, (46) is similar to the baryonic equation derived in three-dimensional QCD [12,13].

Equation (46) can be regarded as the eigenvalue problem, for three identical particles with parton-x coordinates, moving in a box $0 \le x_i \le 1$. If one naively substitutes the potential by vanishing (Dirichlet) boundary condition $\varphi_n(x_i = 0, 1) = 0$, the eigenstates are standing waves, e.g.

$$\varphi_n[x] \approx 2^{\frac{3}{2}}(\sin(n_1\pi x_1)\sin(n_2\pi x_2)\sin(n_3\pi x_3)) \quad (47)$$

with eigenvalues

$$M_n^2 \approx 2\pi\sigma_T(|n_1| + |n_2| + |n_3|) \quad (48)$$

that Reggeize along the diagonal $n_{1,2,3} = n \gg 1$ as

$$\alpha' M_n^2 \approx 3n. \quad (49)$$

The factor of 3 reflects on the star configuration with three strings.

Unfortunately, this solution is very naive, for several reasons. The most obvious is that the independent quantization of three quarks in a box ignores the important momentum conservation constraint

$$X = x_1 + x_2 + x_3 = 1$$

and therefore contains spurious center of mass motion. As already discussed in the previous section, one can use other coordinates which are center of mass free. In particular, the Jacobi coordinates lead to a problem with *two* particles inside the equilateral triangle.

To solve this problem, we proceed in two steps. First, we unwind the square roots by using the einbein trick once again

$$\sum_{i=1}^{3}\left|\frac{i\partial}{\partial x_i}\right| = \frac{1}{2}\left(\frac{1}{e_{iL}} + e_{iL}\left(\frac{i\partial}{\partial x_i}\right)^2\right) \to \frac{1}{2}\left(\frac{3}{e_L} + e_L\sum_{i=1}^{3}\left(\frac{i\partial}{\partial x_i}\right)^2\right) \quad (50)$$

and assume equal $e_{iL} = e_L$ at the extrema, in the steepest descent approximation. Second, we isolate the center-of-mass coordinate, using Jacobi coordinates (18). The 3-particle Laplacian in those coordinates is the sum of a 2-particle reduced Laplacian, plus derivative of the center-of-mass variable

$$\sum_{i=1}^{3}\left(\frac{i\partial}{\partial x_i}\right)^2 = \left(\frac{i\partial}{\partial\lambda}\right)^2 + \left(\frac{i\partial}{\partial\rho}\right)^2 + 3\left(\frac{i\partial}{\partial X}\right)^2. \quad (51)$$

For fixed center of mass $X = 1$, (18) maps the confining box region $B = [0, 1]^3$ for the coordinates x_i, to an equilateral triangle $\Sigma(x)$ of side $L = \sqrt{2}$, with corners located at

$$(\lambda, \rho) = \left(-\sqrt{\frac{2}{3}}, 0\right), \left(\frac{1}{\sqrt{6}}, \frac{1}{\sqrt{2}}\right), \left(\frac{1}{\sqrt{6}}, -\frac{1}{\sqrt{2}}\right).$$

The corners correspond to one particle carrying all the momentum, with the two others at rest.

The eigensystem of the first two terms in the Laplacian (now free from the center of mass motion) amounts to solving

$$-\left(\frac{\partial^2}{\partial\lambda^2} + \frac{\partial}{\partial\rho^2}\right)\varphi_{m_L,n_L}(\lambda,\rho) = e_{m_L n_L}\varphi_{m_L,n_L}(\lambda,\rho) \quad (52)$$

inside the triangle Σ, with Dirichlet boundary condition $\varphi_{m_L,n_L}(\partial\Sigma) = 0$. Remarkably, although the solutions are not available for generic triangles, they are in fact known for equilateral triangles in closed form, found in [14]. Their existence is due to the finite number of ray reflections, which make a closed set, as explained in Appendix E. The spectrum of the Laplacian is given by

$$e^D_{m_L n_L} = \left(\frac{4\pi}{3L}\right)^2\left(\left(m_L - \frac{n_L}{2}\right)^2 + \frac{3}{4}n_L^2\right) \equiv \tilde{e}^D_{m_L n_L}\pi^2 \quad (53)$$

with integer valued longitudinal quantum numbers m_L, n_L, restricted by $m_L \ge 2n_L$. The states with $m_L > 2n_L$ are doubly degenerate, with normalized eigenstates [14]

$$\begin{aligned}\varphi^{Dc}_{m,n}(\lambda,\rho) = \frac{4}{L3^{\frac{3}{4}}}\Bigg[&\cos\left(\frac{2\pi(2m_L - n_L)\rho}{3L}\right)\sin\left(\frac{2\pi n_L\tilde{\lambda}}{\sqrt{3}L}\right)\\ &- \cos\left(\frac{2\pi(2n_L - m_L)\rho}{3L}\right)\sin\left(\frac{2\pi m_L\tilde{\lambda}}{\sqrt{3}L}\right)\\ &+ \cos\left(\frac{2\pi(m_L + n_L)\rho}{3L}\right)\sin\left(\frac{2\pi(m_L - n_L)\tilde{\lambda}}{\sqrt{3}L}\right)\Bigg]\\ \varphi^{Ds}_{m,n}(\lambda,\rho) = \frac{4}{L3^{\frac{3}{4}}}\Bigg[&\sin\left(\frac{2\pi(2m_L - n_L)\rho}{3L}\right)\sin\left(\frac{2\pi n_L\tilde{\lambda}}{\sqrt{3}L}\right)\\ &- \sin\left(\frac{2\pi(2n_L - m_L)\rho}{3L}\right)\sin\left(\frac{2\pi m_L\tilde{\lambda}}{\sqrt{3}L}\right)\\ &- \sin\left(\frac{2\pi(m_L + n_L)\rho}{3L}\right)\sin\left(\frac{2\pi(m_L - n_L)\tilde{\lambda}}{\sqrt{3}L}\right)\Bigg]\end{aligned} \quad (54)$$

with $\tilde{\lambda} = \lambda + L/\sqrt{3}$. Their symmetry properties include e.g. ρ mirror symmetry

$$\varphi^{Dc,s}_{m_L,n_L}(\lambda,-\rho) = \pm\varphi^{Dc,s}_{m_L,n_L}(\lambda,\rho). \tag{55}$$

The Dirichlet states with $m_L = 2n_L$ are nondegenerate, with normalized eigenstates [14]

$$\varphi^{D}_{2n_L,n_L}(\lambda,\rho) = \frac{2^{\frac{3}{2}}}{L3^{\frac{3}{4}}}\left[2\cos\left(\frac{2\pi n_L\rho}{L}\right)\sin\left(\frac{2\pi n_L\tilde{\lambda}}{\sqrt{3}L}\right) - \sin\left(\frac{4\pi n_L\tilde{\lambda}}{\sqrt{3}L}\right)\right]. \tag{56}$$

Since (54)–(56) are separable in (λ,ρ) and harmonic, they are readily seen to solve (51). The proof that these solutions form an orthonormal set on the triangle is nontrivial, but we checked a number of cases explicitly. Implicitly, it follows from the observation that the mode number following from (53) saturates the so-called Weyl area rule [14].

We identify the ground state from the tower of states (56) with $n_L = 1$, and its radial excitations with $n_L > 1$. In Fig. 7 we show the probability distributions for $n_L = 1, 2$.

These states are shown to Reggeize below. We further note that (56) can be recast as three standing waves with three "momenta" $\tilde{k}$

$$\varphi^{D}_{2n_L,n_L}(\lambda,\rho) = \frac{2^{\frac{7}{2}}}{L3^{\frac{3}{4}}}\sin\left(\frac{2\pi n_L\tilde{k}_0}{\sqrt{3}L}\right)\sin\left(\frac{\pi n_L\tilde{k}_+}{\sqrt{3}L}\right)\sin\left(\frac{\pi n_L\tilde{k}_-}{\sqrt{3}L}\right) \tag{57}$$

in the triangular domain limited by the sides

$$\tilde{k}_0 = \sqrt{3}L/2, \qquad \tilde{k}_\pm = \tilde{\lambda} \pm \sqrt{3}\rho = 0.$$

Remarkably, in the original x-Bjorken coordinates the standing waves (57) are identical to those in (47), for fixed $X = x_1 + x_2 + x_3 = 1$, i.e.

$$\varphi^{D}_{2n_L,n_L}(x_1,x_2,x_3) = (-1)^{n+1}\frac{2^3}{X3^{\frac{3}{4}}}\sin\left(\frac{n_L\pi x_1}{X}\right)\sin\left(\frac{n_L\pi x_2}{X}\right)\sin\left(\frac{n_L\pi x_3}{X}\right). \tag{58}$$

[This observation perhaps allows for the extension of the Dirichlet standing states and their excitations, to the states of more exotic hadrons with $N > 2$ compact multiquark content—tetraquarks, pentaquarks, hexaquarks

$$\varphi^{D}_{n_L}(x_1,\ldots,x_N) = \frac{C_N}{X}\prod_{i=1}^{N}\sin\left(\frac{n_L\pi x_i}{X}\right) \tag{59}$$

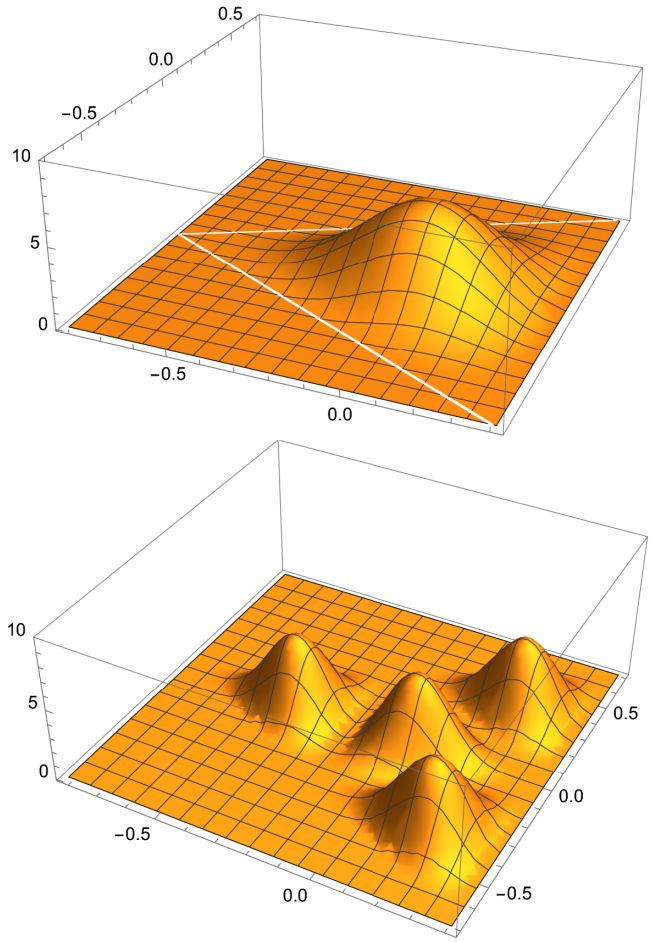

FIG. 7. Probability distribution $|\phi^{D}_{2n_L,n_L}|^2$ for $n_L = 1$ (top) and $n_L = 2$ (bottom) in the λ, ρ plane, with manifest mirror symmetry in ρ.

with $X = \sum_{i=1}^{N} x_i$, and the normalization C_N fixed by the polygonal volume, set by the longitudinal momentum constraint $X = 1$. The meson case with $N = 2$, of course requires a single standing wave, as we used in our previous papers.]

Using (53), the contribution of the Laplacian to the baryon spectrum is

$$\Delta M^2_{m_L n_L} \approx 2\pi\sigma_T\sqrt{3\tilde{e}^{D}_{m_L n_L}} \approx \left(\frac{4}{\sqrt{6}}\right)\left(2\pi\sigma_T\left(\left(m_L - \frac{n_L}{2}\right)^2 + \frac{3}{4}n_L^2\right)^{\frac{1}{2}}\right). \tag{60}$$

For large quantum numbers, it Reggeizes into a linear dependence. For the ground state and its radial excitations series, with $m = 2n$ in (56), its contribution to the spectrum can be compared to the conventional Regge trajectory of the mesons $n = \alpha' M^2$ with $\alpha' = 1/2\pi\sigma_T$

$$\alpha'\Delta M^2_{2n_L,n_L} \approx 2\sqrt{2}n_L. \tag{61}$$

There is an additional factor of $2\sqrt{2} \approx 2.83$ to be also compared with the Regge slope from the spurious spectrum (49), where this factor is just 3, the number of strings.

Let us add the following consideration. Although the "cup" potential $V = \sum m_Q^2/x_i$ was not yet included, its very existence—especially for heavy masses $m_Q^2/2\sigma_T \gg 1$—motivated us to look at standing waves that vanish at the cup's boundaries. In the opposite limit of light quarks $m_Q^2/\sigma_T \leq 1$ we can ignore the confining potential as a small perturbation, and thus ignore its end-point constraint. (Recall that m_Q is not the "Lagrangian" quark mass but an effective one, including the constituent quark mass. So even for light quarks $m_Q \sim 350\,\mathrm{MeV}$, while $\sqrt{\sigma_T} \approx 400\,\mathrm{MeV}$, this limit may be of academic interest only.)

In this case, it is perhaps more appropriate to use free end-point or Neumann boundary conditions

$$\varphi'_{n_L}(x_i = 0, 1) = 0$$

so as to minimize the *kinetic* contribution for the excited states. Again, the eigenstates free of center-of-mass motion can be sought using also the ray reflection method, as we suggest in Appendix E.

In particular, the Neumann analog of the tower of Dirichlet standing states (57) built on the ground state is readily found as

$$\varphi^N_{2n_L,n_L}(\lambda,\rho) = \frac{2^{\frac{7}{2}}}{L3^{\frac{3}{4}}}\cos\left(\frac{2\pi n_L\tilde{\lambda}}{\sqrt{3}L}\right)\cos\left(\frac{\pi n_L\tilde{\lambda}_+}{\sqrt{3}L}\right)\cos\left(\frac{\pi n_L\tilde{\lambda}_-}{\sqrt{3}L}\right) \quad (62)$$

or equivalently in x-Bjorken

$$\varphi^N_{2n_L,n_L}(x_1,x_2,x_3) = (-1)^{n_L}\frac{2^3}{X3^{\frac{3}{4}}}\cos\left(\frac{n_L\pi x_1}{X}\right)\cos\left(\frac{n_L\pi x_2}{X}\right)\cos\left(\frac{n_L\pi x_3}{X}\right) \quad (63)$$

with $X = 1$ subsumed. The solutions (62) satisfy Neumann boundary conditions in the triangular domain by inspection, with the same spectrum and Regge trajectory as Dirichlet for $m_L = 2n_L$, i.e. $e^N_{2n_L,n_L} = e^D_{2n_L,n_L}$ but with $n_L = 0$ *a priori* allowed.

D. Spectrum of the diagonal part of the Hamiltonian H_0

Our light-front Hamiltonian contains three parts,

$$H_{LF} \approx H_{0\perp} + H_{0x_i} + \tilde{V}_{LF}.$$

The first two are transverse oscillator and longitudinal triangular cup: for both of them we managed to find their complete set of eigenfunctions. The remaining residual part is not amenable to analytic integration and will be treated numerically. Also we use the einbein trick to get rid of the square roots in the confining term

$$H_{LF} \approx \sum_{i=1}^{3}\left(\frac{k_{i\perp}^2 + m_Q^2}{x_i} + \sigma_T\left(3a + \frac{1}{a}\sum_{i=1}^{3}(|i\partial/\partial x_i|^2 + (3m_Q)^2 b_{i\perp}^2)\right)\right) \quad (64)$$

with $M \approx 3m_Q$ used on the right-hand side to close the mass squared operator. Again, we assumed equal einbeins $a_i \to a$ in (64) by steepest descent. To the first kinetic term we add and subtract its value at $x_i = \frac{1}{3}$, producing an oscillator with fixed frequency, and a residual potential $\tilde{V}$ which is close to zero at the center of the triangular cup.

In terms of the Jacobi coordinates, the diagonalizable part reads

$$H_{0LF} = 3(\vec{p}_\rho^{\,2} + \vec{p}_\lambda^{\,2} + 3m_Q^2) + \frac{\sigma_T}{a}(|i\partial/\partial\lambda|^2 + |i\partial/\partial\rho|^2 + (3m_Q)^2(\vec{b}_\lambda^{\,2} + \vec{b}_\rho^{\,2})) \quad (65)$$

where all the vectors are in the transverse plane, and $\vec{b}_\lambda, \vec{b}_\rho$ are coordinates conjugate to the corresponding momenta. To elucidate the dependence on a we rewrite it as

$$M_0^2(n_\lambda,n_\rho,n_L,m_L) = (3m_Q)^2 + \frac{\sigma_T}{\sqrt{a}}M_\perp^2(n_\lambda,n_\rho) + \frac{\sigma_T}{a}M_L^2(m_L,n_L) + 3\sigma_T a \quad (66)$$

with

$$M_L^2(n_L,m_L) = e^D_{n_L,m_L}, \qquad M_\perp^2(n_\lambda,n_\rho) = \frac{6\sqrt{3}m_Q}{\sqrt{\sigma_T}}(n_\lambda + n_\rho + 2). \quad (67)$$

The einbein in (66) minimizes the squared mass and is solution to the quartic Ferrari equation

$$6\sqrt{a}^4 - M_\perp^2\sqrt{a} - 2M_L^2 = 0.$$

For large longitudinal quantum numbers $n_L, m_L \gg 1$ the squared mass Reggeizes

$$M_0^2 \approx 2\sqrt{3}\sigma_T M_L$$

as we noted earlier. However, for large transverse quantum numbers $n_\lambda, n_\rho \gg 1$ the squared mass does not,

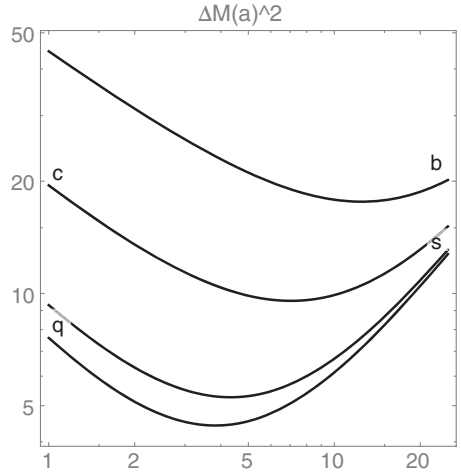

FIG. 8. The lowest eigenvalue of H_{0LF} in GeV^2 versus the (dimensionless) "einbine parameter" a, for b, c, s, q quarks. Using this plot we perform the minimization in a.

$$M_0^2 \approx 18\sigma_T \left(\frac{M_\perp^2}{6\sigma_T}\right)^{\frac{2}{3}}. \tag{68}$$

Recall that the results following from H_{0LF} are still to be modified by the additional residual contributions, stemming from $\tilde{V}_{LF}$ to be added below, but which are independent of our variational parameter a. Therefore the minimization over a can already be performed numerically. With our standard values for the string tension $\sigma_T = (0.4\ \text{GeV})^2$, and quark masses b, c, s, q, we show in Fig. 8 the dependence on a of the lowest eigenvalue for each species.

VI. THE NONFACTORIZABLE POTENTIAL $\tilde{V}$

The nonfactorizable part of the potential is

$$\tilde{V} = \frac{\vec{p}_1^{\,2} + m_Q^2}{x_1} + \frac{\vec{p}_2^{\,2} + m_Q^2}{x_2} + \frac{\vec{p}_3^{\,2} + m_Q^2}{x_3} - 3(\vec{p}_1^{\,2} + \vec{p}_2^{\,2} + \vec{p}_3^{\,2}) - 9m_Q^2. \tag{69}$$

Using the Jacobi coordinates for the transverse and longitudinal momenta, we get

$$\begin{aligned}\tilde{V} = -((&3(-2p_\lambda p_\rho(\sqrt{6}-6\lambda)\rho + 9m_Q^2(2\lambda^2+\sqrt{6}\lambda^3 \\ &+ 2\rho^2 - 3\sqrt{6}\lambda\rho^2) + p_\lambda^2(9\lambda^2 + 3\sqrt{6}\lambda^3 + 3\rho^2 \\ &+ \sqrt{6}\lambda(1-9\rho^2)) + p_\rho^2(3\lambda^2 + 3\sqrt{6}\lambda^3 + 9\rho^2 \\ &- \sqrt{6}\lambda(1+9\rho^2)))) \\ &\times \left(\frac{1}{-2 + 9\lambda^2 + 3\sqrt{6}\lambda^3 + 9\rho^2 - 9\sqrt{6}\lambda\rho^2}\right).\end{aligned} \tag{70}$$

For zero orbital motion, the two oscillators are independent, and the term $\langle p_\lambda p_\rho \rangle$ vanishes on average. $\langle p_\lambda^2 \rangle$ and $\langle p_\rho^2 \rangle$ are directly related to the number of quanta n_λ, n_ρ, and so one has to calculate only the matrix entries in terms of all possible longitudinal quantum numbers $\langle n_L, m_L|\tilde{V}|n'_L m'_L\rangle$, see Appendix F.

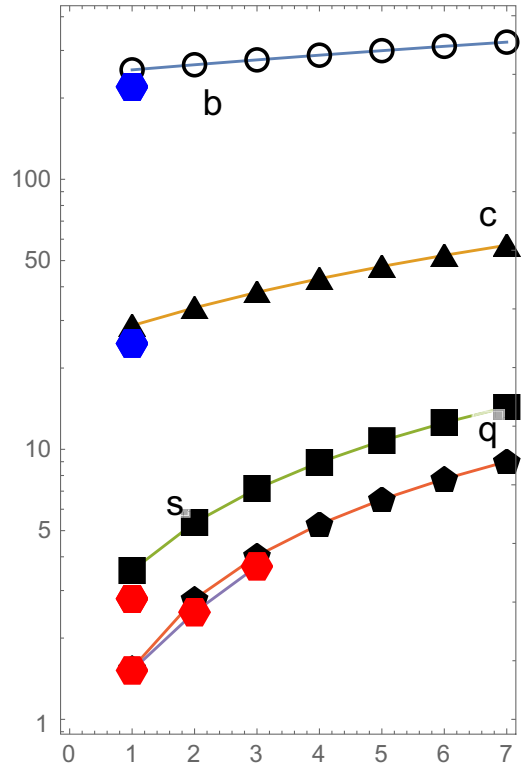

FIG. 9. Squared masses of baryons $M^2_{n+1}(Q, \frac{3}{2})$ in GeV^2 versus the principal quantum number $n+1 = 1..7$. The black circles, triangles, squared, and pentagons are results of our calculations for the flavors b, c, s, q. The red hexagons are the experimental values of three Δ^{++} and one Ω^- masses, from PDG. The two blue hexagons are model predictions for masses of ccc and bbb baryons, from Table I.

A. Masses of the states

With the evaluation of the matrix $\tilde{V}$ and its eigenvalues, our technical task is completed. We now can finally carry the calculation of the full eigenvalues—squared masses of the flavor symmetric baryons, for the four quark flavors b, c, s, q. We keep here longitudinal quantum numbers to their lowest values $n_L = 1$, $m_L = 2$, and assume that the transverse oscillators are excited as a function of a single $n = (n_\rho + n_\lambda)/2$.

Our results for squared masses are shown in black symbols in Fig. 9. For comparison, we show the experimental masses in red hexagons. The blue hexagons are available model predictions for ccc and bbb baryons. Since a constant in LF Hamiltonian remains undefined, we fixed one constant for all masses, so that the mass of the uuu baryon Δ^{++} is set to experimental one. For definiteness, the plots correspond to effective masses of u, s, c, b quarks to

be 0.28, 0.45, 1.5, 4.8 GeV, respectively, not specially fitted to this plot but inherited from meson studies.

Finally, let us remind the reader that all the calculations were done for traditional star or Y model of confinement. Transition to (perhaps more accurate) Ansatz A leads to the same Hamiltonian with a string tension rescaling (21), downwards by about 13% like one has observed it in static potentials.

VII. WAVE FUNCTIONS OF THE STATES

Our main results are not the masses of the $\frac{3}{2}^+$ states and their radial excitations, but their corresponding wave functions. The ground states in all channels have a transverse momentum dependence that is about Gaussian, e.g. $\psi(p_\perp) \sim \exp(-\beta^2 p_\perp^2/2)$. The scale parameter β is related to the mass and frequency of the effective oscillator μ, ω,

$$\beta = \sqrt{\mu\omega} = \left(\frac{a}{3m_Q^2\sigma_T}\right)^{\frac{1}{4}}. \tag{71}$$

The mean square of the transverse momentum is approximately

$$\langle p_\perp^2\rangle \approx \beta^{-2} \approx 0.942, 0.466, 0.183, 0.104\ (\mathrm{GeV}^2) \tag{72}$$

for the b, c, s, q $3/2^+$ single-flavor baryons.

The longitudinal wave functions for heavy quark masses m_Q are defined mainly by the $O(m_Q^2)$ part of the potential $\tilde{V}$. They are discussed in Appendix E, and illustrated in Fig. 12 by the solid black line. In general, since the Hamiltonian is H_0 plus $\tilde{V}$, the wave functions lie between their eigenfunctions, or between the solid and dashed line in Fig. 12. We note that the difference is mostly around the negative maximum of λ, or when x_3 is close to 1. Since the triangle is equilateral and the wave function is symmetric, this implies that the suppression in fact occurs near all three corners of the triangle.

VIII. LONGITUDINAL WAVE FUNCTIONS, FOR TWO-STRING OR V CONFIGURATION

Finally, we now show how the baryon configuration with a "quark-on-junction," or two-string V configuration, once reduced to a longitudinal part, can also be solved. In this configuration, the central quark can be e.g. a heavy one, or it can be a d quark jumping between two us (reminiscent to the 1-folded string [15]). In this case it is more convenient to use another set of coordinates

$$x_1 = \frac{1}{3} + y_1, \quad x_2 = \frac{1}{3} + y_2 - y_1, \quad x_3 = \frac{1}{3} - y_2, \tag{73}$$

which are also canonically conjugate $[y_i, r_i] = i\delta_{ij}$. In those variables the physical domain is an isosceles triangle with corners at $(2/3, 1/3)$, $(-1/3, -2/3)$, $(-1/3, 1/3)$, or half the two-dimensional square.

With this in mind, we can recast (46) as

$$M_n^2\varphi_n[y] = \left(\frac{m_1^2}{\frac{1}{3}+y_1} + \frac{m_2^2}{\frac{1}{3}+y_2-y_1} + \frac{m_3^2}{\frac{1}{3}-y_2} + 2\sigma_T(|i\partial_{y_1}| + |i\partial_{y_2}|)\right)\varphi_n[y]. \tag{74}$$

Using again the einbein trick to make the confining part quadratic, and changing the momenta to derivatives over coordinates, yields a similar eigenvalue problem as that for the star configuration. The only difference is that the cup potential is now an isosceles triangle instead of an equilateral one. Remarkably, the Laplacian problem on it also admits an exact solution, by the eikonal ray construction the same as for the equilateral case. The solutions are the superposition of the symmetric and antisymmetric standing waves on the unit square

$$\varphi^{\pm}_{m_L,n_L}(x_1,x_3) = \sqrt{2}(\sin(m_L\pi x_3)\sin(n_L\pi x_1) \pm \sin(n_L\pi x_3)\sin(m_L\pi x_1)) \tag{75}$$

with $y_{1,2}$ reexpressed in terms of parton $x_{1,3}$ given in (73), and the corresponding eigenvalues

$$e^+_{m_L,n_L} = \pi^2(m_L^2+n_L^2), \quad m_L = n_L \pm 1, \quad n_L \pm 3,$$
$$e^-_{m_L,n_L} = \pi^2(m_L^2+n_L^2), \quad m_L = n_L \pm 2, \quad n_L \pm 4. \tag{76}$$

Equation (75) is symmetric or antisymmetric under the exchange of $x_{1,3}$ (exchange of the u-quarks at the end points), and both vanish for parton-x $x_{1,3} = 0$ and $x_1 + x_3 = 1$ or equivalently $x_2 = 0$, as expected. The lowest state corresponds to $m_L = n_L + 1 = 2$, with a PDF for the u-quark

$$u(x_1) = \int_0^{1-x_1} dx_3 |\varphi^+_{21}(x_1,x_3)|^2 \to \frac{(2\pi^2)^2}{3}(1-x_1)^5 \tag{77}$$

which is again very soft at large parton-x.

The V-string quantum spectrum follows the same reasoning as that for the star baryon, with the result

$$\alpha' M^2_{m_\pm} = (m_+^2 + m_-^2)^{\frac{1}{2}} \tag{78}$$

where $m_\pm = m_L \pm n_L$. Equation (78) Reggeizes with the meson slope of 1 along m_-. These Regge trajectories are the quantum states in correspondence with the classical yo-yo states, noted in [15].

With the inclusion of the "cup potential" induced by the kinetic energy we also solved the problem numerically. The lowest state on this triangle is shown in Fig. 10 (top).

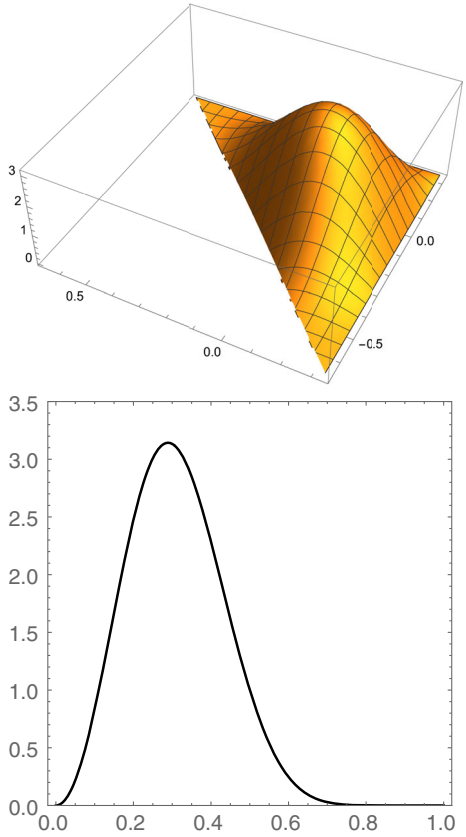

FIG. 10. Top: ground state wave function $\varphi^{+}_{21}(x_1, x_3)$ of the V baryon in (75). Bottom: corresponding PDF for the ground state in (77).

In a standard way we also calculated DAs and PDFs for quarks: due to lack of symmetry, they are different for those in 45° and 90° corner quarks. The PDF for the former is shown in Fig. 10 (bottom), and as one can see it also is way too "soft" at $x \to 1$ as compared to the observed PDF of the nucleon.

IX. CONCLUSIONS

We start by recalling the chief goals of this series of papers, namely to bring together the QCD studies of hadronic spectroscopy and light-front observables—DAs, PDFS, generalized parton distributions (GPDs), etc. The use of the light-front formulation brings in certain issues, but enforces relativistic kinematics, for both the light and heavy quarks, and allows the study of their bound state structure in a single framework.

We believe that hadronic physics should have the same logical and methodical structure, as that in atomic and nuclear physics. Quantum dynamics should be defined by a Hamiltonian, which can be simplified at first but focus on the main physics. For example, in this paper we have included the kinetic term and the confining term only, leaving the more complicated contributions (Coulomb and spin-dependent forces) for next studies.

Once the Hamiltonian is defined, its diagonalization yields physical states, which automatically possess such basic properties as mutual orthogonality. This part of the problem is rather technical and took most of this paper. We have shown that one can do so, either by using diagonalization in a certain basis set, or numerically solve for wave functions (as we did for longitudinal ones). Any wave function is complete, in the sense that one can calculate any observable from it, say various PDFs, GPDs, and form factors by standard general formulas. Of course, those are defined at a normalization scale with *low resolution*, at which gluons and antiquarks are suppressed. Comparison with data at a high resolution scale of experiments should include their evolution by well-developed perturbative QCD tools.

In our attempts to *derive* the light-front Hamiltonian H_{LF} we have focused on the nonperturbative interquark interaction. We started by relating the lattice data to a few simple models of confinement, Y, V, and A models. They follow from relativistic QCD strings (flux tubes) with a linear dependence on the size of the baryon. Then we performed our own evaluation of the three-quark potentials from Wilson line correlators, based on a semiclassical model of the Euclidean QCD vacuum using a dense instanton liquid. We find a reasonably good agreement between the results and lattice numerical data. We also see that out of three empirical models, the Ansatz A seems to be the closest to these potentials.

The important distinctions between our approach and other versions of H_{LF} in the literature are, among others, the following:

(1) H_{LF} is derived from established QCD lattice facts.
(2) We do not rush to fit any parameters to the experimental data but use only standard values for the effective quark masses, and the string tension σ_T.
(3) We do not even start with the nucleon, for which obviously there is large set of experimental data, but study single-flavor baryons because they should not have strong diquark clustering which is known to be flavor-antisymmetric.
(4) We do not focus on only the ground state but consider several excited states in each quark channel, so that the dependence on principal and orbital quantum numbers can be available. It is imperative that the Hamiltonian used does have reasonable predictions for many states, at least they approximately reproduce the expected Regge behavior.

This paper is mostly technical in nature, in it we showed *how one can solve the quantum mechanical problem* of three identical quarks, given their interaction by a confining string. Unlike other approaches in the light-front literature, we use as many degrees of freedom as needed: six Jacobi coordinates/momenta for three-quark baryons. There is no need to "subtract spurious center of mass motion." We do quantum mechanics in momentum representation, and

therefore, in the longitudinal direction we show how to solve a Schrödinger-like equation on a physical triangle. The "unfactorizable" potential is defined, set into its minimal form, and its effect on the wave functions is evaluated by diagonalization in the appropriate basis or by numerical solution for a subset of degrees of freedom.

This paper focuses on flavor symmetric (QQQ) baryons with maximal spin $\frac{3}{2}$, the most symmetric setting to start with. Perturbative Coulomb forces—believed to be important for heavy quarks—are not yet included, as well as spin-dependent forces. Effects related to a 't Hooft instanton-induced Lagrangian—believed to be important for light quarks and contributing to "diquark" correlations—will be discussed in the sequel of this series [4].

ACKNOWLEDGMENTS

This work is supported by the Office of Science, U.S. Department of Energy under Contract No. DE-FG-88ER40388.

APPENDIX A: AVERAGING OVER THE $SU(3)$ ROTATIONS

The color averaging over the unitary matrices can be carried using the Weingarten coefficients

$$\begin{aligned}\langle U^{a_1}_{c_1} U^{\dagger b_1}_{d_1} U^{a_2}_{c_2} U^{\dagger b_2}_{d_2} U^{a_3}_{c_3} U^{\dagger b_3}_{d_3}\rangle_U &= +\frac{(N_c^2-2)}{N_c(N_c^2-1)(N_c^2-4)}\sum_{n=1}^{3!}\delta^{a_1a_2a_3}_{(d_1d_2d_3)_n}\delta^{c_1c_2c_3}_{(b_1b_2b_3)_n}\\ &-\frac{1}{(N_c^2-1)(N_c^2-4)}\\ &\times\sum_{n=1}^{3!}\delta^{a_1a_2a_3}_{(d_1d_2d_3)_n}(\delta^{c_1c_2c_3}_{(b_2b_1b_3)_n}+\delta^{c_1c_2c_3}_{(b_1b_3b_2)_n}+\delta^{c_1c_2c_3}_{(b_3b_2b_1)_n})\\ &+\frac{2}{N_c(N_c^2-1)(N_c^2-4)}\\ &\times\sum_{n=1}^{3!}\delta^{a_1a_2a_3}_{(d_1d_2d_3)_n}(\delta^{c_1c_2c_3}_{(b_3b_1b_2)_n}+\delta^{c_1c_2c_3}_{(b_2b_3b_1)_n})\end{aligned} \tag{A1}$$

where the shorthand notation used

$$\delta^{a_1a_2a_3}_{(d_1d_2d_3)_n}\equiv\sum_{n=1}^{3!}(\delta^{a_1}_{d_1}\delta^{a_2}_{d_2}\delta^{a_3}_{d_3}+\text{perm.}) \tag{A2}$$

refers to the product of three Kroneckers in the sum over the $n!$ permutations of the permutation group S_3. Inserting (A1) into (9), and using the identities in [16], we have

$$\begin{aligned}&+\left[\left(\frac{2}{N_c}\right)^3 c_1c_2c_3\right]\delta^{a_1}_{b_1}\delta^{a_2}_{b_2}\delta^{a_3}_{b_3}\\ &+\left[\frac{1}{2N_c(N_c^2-1)}c_1\mathrm{Tr}(-is_2\tau\cdot n_2\lambda_2^A)\mathrm{Tr}(-is_3\tau\cdot n_3\lambda_3^A)\right]\delta^{a_1}_{b_1}(\lambda_2^B)^{a_2}_{b_2}(\lambda_3^B)^{a_3}_{b_3}+2\text{ perm.}\\ &+\left[\frac{N_c}{8(N_c^2-1)(N_c^2-4)}d^{IJK}\mathrm{Tr}(-is_1\tau\cdot n_1\lambda_1^I)\mathrm{Tr}(-is_2\tau\cdot n_2\lambda_2^J)\mathrm{Tr}(-is_3\tau\cdot n_3\lambda_3^K)\right]d^{ABC}(\lambda_1^A)^{a_1}_{b_1}(\lambda_2^B)^{a_2}_{b_2}(\lambda_3^C)^{a_3}_{b_3}\\ &+\left[\frac{8}{8N_c(N_c^2-1)}f^{IJK}\mathrm{Tr}(-is_1\tau\cdot n_1\lambda_1^I)\mathrm{Tr}(-is_2\tau\cdot n_2\lambda_2^J)\mathrm{Tr}(-is_3\tau\cdot n_3\lambda_3^K)\right]f^{ABC}(\lambda_1^A)^{a_1}_{b_1}(\lambda_2^B)^{a_2}_{b_2}(\lambda_3^C)^{a_3}_{b_3}\end{aligned} \tag{A3}$$

which is explicit in terms of the invariants of $SU(3)_c$. Furthermore, the $SU(2)_c$ color structure of the instanton is not enough to support the last two terms with f, d structure constants in (A3).

APPENDIX B: THE EINBEIN TRICK

For completeness, we briefly recall the use of the einbein trick. Consider an expression (operator X) of the form

$$X\to\frac{1}{2}\left(aX^2+\frac{1}{a}\right) \tag{B1}$$

with a variational parameter a. The right-hand side can be readily used in a Hamiltonian. Noting that the right-hand side has a minimum as a function of a, and that its value at the minimum is the left-hand side, the latter follows from the former.

This trick is used in Sec. III B to eliminate the square root of the relativistic kinetic energy $\sqrt{p^2+m^2}$ in the c.m. frame, and in the rest of the paper by changing from linear confinement to its quadratic form.

APPENDIX C: LAPLACIAN OPERATOR AND BASIS FUNCTIONS FOR s, t MAP (35)

Given a coordinate mapping $y^m=(s,t,u)$, there is a well-defined procedure for the rewriting of the Laplacian in differential geometry, using the metric tensor g,

$$g = \begin{bmatrix} 1/8(u^2+2tu^2+t^2u^2) & 1/8(su^2+stu^2) & 1/8(su+2stu+st^2u) \\ 1/8(su^2+stu^2) & 1/8(3u^2+s^2u^2) & 1/8(-u+s^2u+3tu+s^2tu) \\ 1/8(su+2stu+st^2u) & 1/8(-u+s^2u+3tu+s^2tu) & 1/8(3+s^2-2t+2s^2t+3t^2+s^2t^2) \end{bmatrix}. \quad \text{(C1)}$$

The covariant Laplacian is given by the expression

$$L = \frac{1}{\sqrt{g}}\frac{\partial}{\partial y^m}\sqrt{g}g^{mn}\frac{\partial}{\partial y^n} \quad \text{(C2)}$$

where g^{mn} is the inverse matrix to g_{mn} in (C1), and $g = det(g_{mn})$. Only the determinant is simple enough to be quoted here

$$g = \frac{u^4}{64}(1+t)^2.$$

The full expression for the Laplacian is involved and will not be given here. Fortunately one of the variables—the "scale" u—can be set to one, and all derivatives over it neglected. Then the result takes the somehow simple form

$$L[\phi] = \frac{1}{(1+t)^2}\left(+2(1+t)^2(-1+3t)\frac{\partial\phi(s,t)}{\partial t} + (3+4t+2t^2+4t^3+3t^4)\frac{\partial^2\phi(s,t)}{\partial t^2} + 16s\frac{\partial\phi(s,t)}{\partial s} + (-8s+8st^2)\frac{\partial^2\phi(s,t)}{\partial t\partial s} + (8+8s^2)\frac{\partial^2\phi(s,t)}{\partial s^2}\right). \quad \text{(C3)}$$

The physical wave functions must have boundary conditions that are consistent with finiteness of the Laplacian. (And the "nonfactorizable" potential $\tilde{V}$, which is proportional to $1/(x_1x_2x_3)$ and thus singular at the boundaries.) Therefore all wave functions can be supplied with some suppression factors, which for this map may take a factorized form

$$\Psi(s,t) = (1-s^2)(1-t)^a(1+t)^b\Phi(s,t)$$

with some parameters a, b ensuring finiteness of all matrix elements. The remaining nonsingular function $\Phi(s,t)$ can be conveniently expressed as products of Jacobi polynomials $P_n^{A,B}(s)P_{n'}^{C,D}(t)$, with indices A, B, C, D related to a, b and the invariant measure $\sqrt{g}$.

APPENDIX D: BASIS FUNCTIONS FOR TRANSVERSE MOMENTA

The LFWFs part depends on two (Jacobi) transverse momenta (16) $\vec{\rho}_\perp, \vec{\lambda}_\perp$, via a double set of 2d Harmonic oscillator wave functions. Those are the same as the ones we used in our previous papers for mesons. They can be written in compact form using generalized Laguerre polynomials

$$\psi_{n,m}(p_\perp,\beta) = \frac{\sqrt{2}}{2\pi}\beta\sqrt{\frac{n!}{(n+|m|)!}}e^{-p_\perp^2\beta^2/2+im\phi} \times (p_\perp\beta)^{|m|}L_n^{|m|}(\beta^2p_\perp^2) \quad \text{(D1)}$$

where $\vec{p}_\perp$ stands for $\vec{\rho}$ or $\vec{\lambda}$. The value of beta comes from H_0 as discussed in Sec. V D.

APPENDIX E: CONFINED QUANTUM WAVES IN AN EQUILATERAL TRIANGLE

In this appendix, we outline the derivation of the confined quantum waves by an equilateral triangle, which leads to (54)–(56), as solutions to the two-dimensional Shrödinger equation (51), with the result given in [14]. In the absence of the confining boundary conditions, the solutions are separable in harmonic waves $e^{\pm ik\cdot r}$, with $\vec{k} = (k_x, k_y)$ a two-dimensional real wave vector in the (x,y) coordination used in [14] (or $x = \rho + L/2$ and $y = -\lambda + L/2\sqrt{3}$ in our coordination) as illustrated in Fig. 11. The triangle confines the waves, by enforcing the wave amplitudes to vanish at the triangle edges. We now explain how.

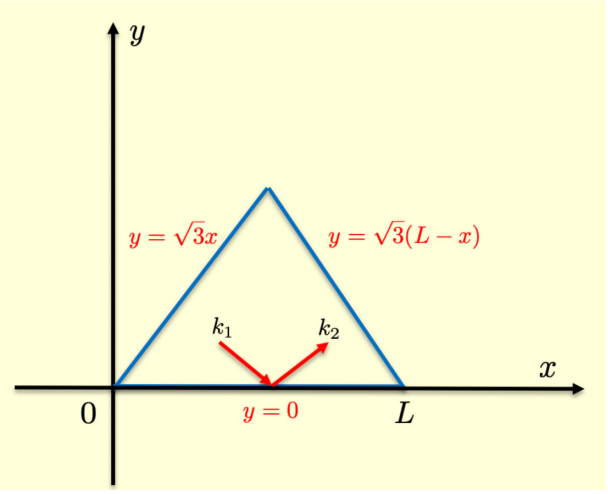

FIG. 11. Equilateral triangle used for the light-ray construction, with the $k_{1,2}$ rays shown. See text.

Following the construction outlined in [14], consider the equilateral triangle with corners $(x,y)=(0,0),(0,L),(L/2,\sqrt{3}L/2)$ in the labeling of [14] [our triangular domain in (λ,ρ) followed by the mapping quoted above]. A ray in the equilateral triangle with arbitrary wave-vector $\vec{k}$ can undergo six distinct reflections before emerging parallel to itself (arbitrary triangles would not close under reflection). Each pair of rays at the triangle side fulfills the null amplitude condition. As a result, we can pair the rays at each side, to generate the solution to (51) with triangular confining walls, by superposition thanks to the linearity of the Sturm-Liouville problem. Six ray reflections map the equilateral triangular phase space onto that of a torus phase space and close the reflection cycle. We note that half the equilateral triangle, and the right-angle isosceles triangle (half of a square) are two other triangular domains, with a closed reflection phase space as well. (Incidentally, these are also the triangles for which the Coulomb problem using the image construction closes with a finite number of images.)

Let $\vec{k}_{i=1,\ldots,6}$ be the six reflected wave vectors, initiated by the harmonic solution with $\vec{k}_1=(k_x,k_y)$, that close the reflection cycle in the equilateral triangle. The reflection of $\vec{k}_1$ by the wall at $y=0$ generates the reflected wave-vector $\vec{k}_2=(k_x,-k_y)$. By construction, the harmonic combination

$$(e^{-ik_1\cdot r}-e^{-ik_2\cdot r})(x,y=0)=0 \tag{E1}$$

solves (51) since $k_1^2=k_2^2$ and satisfies the null condition on the triangle side $y=0$. The next pair of reflections on the triangle side $y=\sqrt{3}x$ yields the pair of wave vectors $\vec{k}_3=-\frac{1}{2}(k_x+\sqrt{3}k_y,-\sqrt{3}k_x+k_y)$ and $\vec{k}_4=-\frac{1}{2}(k_x-\sqrt{3}k_y,-\sqrt{3}k_x-k_y)$. The superposition (E1) with the substitution $4,1,2\to 3$, again solves (51) since $k_3^2=k_4^2$ and satisfies the null condition on the triangle side $y=\sqrt{3}x$. The same reasoning applies to the last pair of reflections back at the wall at $y=0$, with $\vec{k}_5=-\frac{1}{2}(k_x-\sqrt{3}k_y,\sqrt{3}k_x+k_y)$ and $\vec{k}_6=-\frac{1}{2}(k_x+\sqrt{3}k_y,\sqrt{3}k_x-k_y)$, followed by the substitution $1,2\to 5,6$ in (E1). The quantization of the wave vectors in (54)–(56) with Dirichlet boundaries follow by the null condition of

$$\varphi_k^D(x,\sqrt{3}(L-x)) = \left(\sum_{i=1}^{6}(-1)^{i+1}e^{-ik_i\cdot r}\right)(x,\sqrt{3}(L-x))=0 \tag{E2}$$

on the last triangular side $y=\sqrt{3}(L-x)$. Note that all wave contributions carry ± 1 weight by reflection symmetry. This is the solution derived in [14], and used in our analysis, after pertinent rotation and translation of the equilateral triangle quoted here.

Finally, we note that the Neumann boundary conditions on the equilateral triangle can be enforced using a similar reasoning to that for Dirichlet, but with all ray contributions carrying the same sign, and (E2) changed to

$$\varphi_k^N(x,\sqrt{3}(L-x)) = \left(\sum_{i=1}^{6}e^{-ik_i\cdot r}\right)(x,\sqrt{3}(L-x))=0. \tag{E3}$$

APPENDIX F: THE NONFACTORIZABLE POTENTIAL $\tilde{V}$

The expression of this potential in Jacobi coordinates has been given in (70), and here we discuss its matrix elements. For that we use the family of states (56), with a single quantum number n_L.

For definiteness, we only give the matrix elements proportional to p_λ^2, p_ρ^2 (the ones proportional to m_Q^2 are similar). Specifically, the upper 4×4 part is

$$\frac{\langle n_{L1}|\tilde{V}|n_{L2}\rangle}{p_\lambda^2} = \begin{pmatrix} 2.26289 & 1.90816 & 1.31215 & 0.991796 \\ 1.90816 & 5.75718 & 2.73486 & 2.04179 \\ 1.31215 & 2.73486 & 7.95585 & 3.30115 \\ 0.991796 & 2.04179 & 3.30115 & 9.56256 \end{pmatrix}.$$

Note that it grows strongly with increasing quantum number, and then it decreases away from the diagonal, although rather slowly. Therefore the eigenstates involve strong mixing, and are not very close to the original states (56) (which are eigenstates of the Laplacian in the triangle).

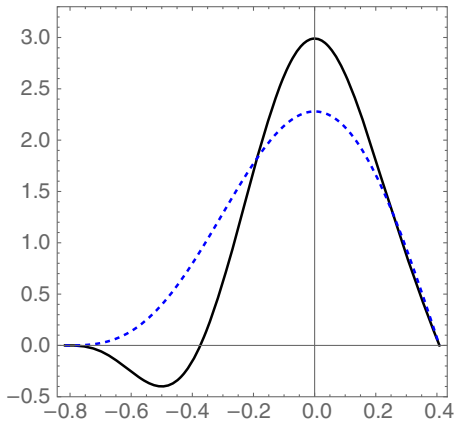

FIG. 12. The eigenfunction (F1) at $\rho=0$ as a function of λ is shown by the solid black curve, to be compared to the lowest standing wave (eigenstate of H_0 for $n_L=1$) as the dashed blue curve (56).

In particular, the eigenvalues of this matrix are 1.42047, 4.14098, 5.98336, 13.9937, somewhat spreading from the diagonal matrix elements. Only the lowest state eigenvector (in the original basis) shows dominance of the lowest states, with strong decrease of the higher state admixture $C_l = 0.920434,\ -0.390426,\ -0.017908,\ -0.00695135$, hence the probabilities $|C_l^2|$ for $n_L > 2$ are negligibly small. Note also that the corrections are all negative. To explain what these corrections do, we show the eigenfunction

$$\psi_{\tilde{V}} = \sum_l C_l \varphi^D_{l,l}(\lambda, \rho) \tag{F1}$$

as a solid black curve in Fig. 12. The dashed blue curve is the exact and lowest standing wave in (56) for $n_L = 1$.

Since the Hamiltonian is a combination of H_0 (thus the Laplacian) and $\tilde{V}$, physical wave functions for the ground state baryons must be *in between* the two curves shown in Fig. 12.

[1] E. Shuryak and I. Zahed, this issue, Phys. Rev. D **107**, 034023 (2023).
[2] E. Shuryak and I. Zahed, this issue, Phys. Rev. D **107**, 034024 (2023).
[3] E. Shuryak and I. Zahed, preceding paper, Phys. Rev. D **107**, 034025 (2023).
[4] E. Shuryak and I. Zahed, following paper, Phys. Rev. D **107**, 034027 (2023).
[5] E. Shuryak, Phys. Rev. D **100**, 114018 (2019).
[6] N. Isgur and G. Karl, Phys. Rev. D **20**, 1191 (1979).
[7] W. Roberts and M. Pervin, Int. J. Mod. Phys. A **23**, 2817 (2008).
[8] J. Bjorken, Report No. FERMILAB-FN-0986-T, 1986.
[9] J. M. Cornwall, Phys. Rev. D **54**, 6527 (1996).
[10] Y. Koma and M. Koma, Phys. Rev. D **95**, 094513 (2017).
[11] Y. A. Simonov, Phys. Lett. B **228**, 413 (1989).
[12] I. Bars, Nucl. Phys. **B111**, 413 (1976).
[13] M. Durgut, Nucl. Phys. **B116**, 233 (1976).
[14] P. Richens and M. Berry, Physica (Amsterdam) **2D**, 495 (1981).
[15] W. A. Bardeen, I. Bars, A. J. Hanson, and R. D. Peccei, Phys. Rev. D **13**, 2364 (1976).
[16] E. Shuryak and I. Zahed, arXiv:2102.00256.